

Delocalization error: The greatest outstanding challenge in density-functional theory

Kyle R. Bryenton¹  | Adebayo A. Adeleke²  | Stephen G. Dale³  |
 Erin R. Johnson^{1,2} 

¹Department of Physics and Atmospheric Science, Dalhousie University, Halifax, Nova Scotia, Canada

²Department of Chemistry, Dalhousie University, Halifax, Nova Scotia, Canada

³Queensland Micro- and Nanotechnology Centre, Griffith University, Nathan, Queensland, Australia

Correspondence

Erin R. Johnson, Department of Chemistry, Dalhousie University, 6274 Coburg Rd, Halifax, Nova Scotia B3H 4R2, Canada.
 Email: erin.johnson@dal.ca

Funding information

Killam Trusts; Natural Sciences and Engineering Research Council of Canada; Australian Research Council, Grant/Award Number: DP200100033

Edited by: Peter R. Schreiner,
 Editor-in-Chief

Abstract

Every day, density-functional theory (DFT) is routinely applied to computational modeling of molecules and materials with the expectation of high accuracy. However, in certain situations, popular density-functional approximations (DFAs) have the potential to give substantial quantitative, and even qualitative, errors. The most common class of error is delocalization error, which is an overarching term that also encompasses the one-electron self-interaction error. In our opinion, its resolution remains the greatest outstanding challenge in DFT development. In this paper, we review the history of delocalization error and provide several complimentary conceptual pictures for its interpretation, along with illustrative examples of its various manifestations. Approaches to reduce delocalization error are discussed, as is its interplay with other shortcomings of popular DFAs, including treatment of non-bonded repulsion and neglect of London dispersion.

This article is categorized under:

Electronic Structure Theory > Density Functional Theory

KEY WORDS

charge transfer, delocalization error, density-functional theory, electron delocalization, self interaction

1 | INTRODUCTION

Kohn-Sham density-functional theory (KS-DFT)¹ is now the workhorse of computational chemistry, solid-state physics, and materials science. Papers proposing some of the most popular functionals constitute 12 of the top 100 most-cited scientific papers, across all fields.² For the majority of chemical systems, DFT methods provide an excellent balance between computational cost and accuracy. They are highly successful in modeling reaction thermochemistry and kinetics, proposing reaction mechanisms, investigating dynamics, modeling solid-state structure, and predicting phase transitions, to list a few examples. However, for certain classes of systems, popular KS-DFT methods have the potential to fail dramatically. One such class of system is those with multireference character,^{3–9} meaning that the wavefunction cannot be well represented by a single electronic configuration (i.e., Slater determinant). Development of DFT methods for multireference systems has been the subject of much recent research,^{10–24} although they are relatively rare in ground-state chemistry.

More commonly, errors are seen for systems with highly delocalized electron densities. The most notable examples are H₂⁺, with its bond length stretched far beyond equilibrium,^{4,25–28} and analogous stretched ions (He₂⁺, Li₂⁺, Ne₂⁺, etc.). However, similar errors have been identified for many other systems, including charge-transfer complexes,^{29–32}

transition states of radical reactions,^{33–38} band gaps of semi-conductors,^{39–44} polarizabilities of long-chain molecules,^{45–48} systems with extended conjugation,^{49–58} halogen and chalcogen bonds,^{59–61} and organic acid/base co-crystals.⁶² These are not the result of separate errors, but rather represent many facets of one single error in common density functionals. This error was originally termed self-interaction error (SIE)⁶³ and discussed in the context of a single electron. However, its definition was later expanded^{64–66} and the more general case is known as delocalization error.⁶⁷ The latter is the more inclusive term, since delocalization error may still affect results that have been corrected for (one-electron) SIE. While many methods have been proposed over the past four decades to limit delocalization error, no one approach is a panacea and research in this area is ongoing.^{6,68–74} Resolving delocalization error almost certainly remains the greatest outstanding challenge in DFT.

In this work, we will review the history of delocalization error, describing three different perspectives on its theoretical underpinnings. We will discuss how this error can be analyzed in terms of density and energy contributions. Further, we will consider the relation between delocalization error and dispersion corrections, and emphasize the importance of obtaining accurate predictions for the right physical reasons. Finally, we will provide a brief survey of some classes of functionals undergoing current development that offer promise in reducing delocalization error.

2 | THEORETICAL BACKGROUND

2.1 | Overview of DFT

In KS-DFT, the energy of a chemical system can be obtained from the electron density and occupied KS orbitals. The total energy is

$$E = T_0 + V_{\text{nuc}} + J_{\text{ee}} + E_{\text{XC}}. \quad (1)$$

T_0 is the noninteracting kinetic energy,

$$T_0 = -\frac{1}{2} \sum_{\sigma} \sum_i \int \psi_{i\sigma}(\mathbf{r}) \nabla^2 \psi_{i\sigma}(\mathbf{r}) d\mathbf{r}, \quad (2)$$

where σ denotes electron spin and the ψ 's are the occupied KS orbitals, assumed to be real. V_{nuc} is the potential energy from electron-nuclear interactions,

$$V_{\text{nuc}} = \sum_{\sigma} \int \rho_{\sigma}(\mathbf{r}) V_{\text{ext}} d\mathbf{r}, \quad (3)$$

where V_{ext} is the external potential from the nuclei and ρ_{σ} is the σ -spin electron density, which can be determined from the real, occupied KS orbitals as

$$\rho_{\sigma}(\mathbf{r}) = \sum_i \psi_i^2(\mathbf{r}). \quad (4)$$

J_{ee} is the classical Coulomb energy for electron–electron interactions,

$$J_{\text{ee}} = \frac{1}{2} \iint \frac{1}{r_{12}} \rho(\mathbf{r}_1) \rho(\mathbf{r}_2) d\mathbf{r}_1 d\mathbf{r}_2, \quad (5)$$

where r_{12} is the electron–electron distance. Finally, E_{XC} is the exchange-correlation energy, which is usually written as a functional of the density and its derivatives. This latter term may be further divided into separate exchange (E_{X}) and correlation (E_{C}) energies.

KS-DFT is exact, in principle, provided that one can employ the exact exchange-correlation functional. However, this functional is unknown and there is no systematic route to obtain it.^{1,75} In practice, various approximations to E_{XC}

are classified by their dependence on the density. The simplest density-functional approximation (DFA) is the local spin-density approximation (LSDA),^{1,63,76–78} where E_{XC} depends only on the density at each point on a real-space grid.⁷⁹ The next most sophisticated DFAs are generalized gradient approximations (GGAs), where E_{XC} depends on the density and its gradient at each point. Many different GGAs have been proposed (B86a,⁸⁰ B86b,⁸¹ PW86,⁸² B88,⁸³ PW91,⁸⁴ PBE,⁸⁵ PBEsol,⁸⁶ etc.) and the choice of GGA is particularly important for describing nonbonded repulsion.^{87–95} GGAs are the standard models employed in solid-state DFT using planewave/pseudopotential codes.

Beyond GGAs, meta-GGAs also include dependence on the kinetic-energy density (τ), and occasionally on the Laplacian of the density as well.^{96–106} Functions of the kinetic-energy density can be used to describe electron delocalization,^{107,108} so meta-GGAs aim to include some correction for self-interaction at close to GGA cost. There are two general philosophies behind the development of meta-GGAs. Many meta-GGAs, most notably M06L¹⁰² and related Minnesota functionals, use power-series expansions of the exchange and correlation energies with empirical parameters fit to thermochemical reference data. Alternatively, others are designed to obey certain physical constraints, including the popular SCAN¹⁰⁵ functional and its recent revision, r²SCAN,¹⁰⁶ with improved numerical stability. While both types tend to perform relatively well for thermochemistry benchmarks such as GMTKN55,^{109,110} use of the more complicated functional forms of meta-GGAs does not necessarily lead to improved accuracy.^{111,112} As we will see, the LSDA, GGAs, and meta-GGAs all have significant inherent delocalization error,^{28,109,113} albeit to differing extents.^{114–117}

Next is the class of hybrid functionals,¹¹⁸ which include the exact exchange energy from Hartree–Fock theory. Global hybrids involve a constant, position-independent mixing of density-functional and exact exchange of the form

$$E_X^{\text{hybrid}} = a_X E_X^{\text{HF}} + (1 - a_X) E_X^{\text{DFA}}, \quad (6)$$

where $0 < a_X < 1$ is the mixing parameter. These are the most commonly used methods in molecular DFT. Hybrids designed for general thermochemistry, such as B3LYP,^{119–121} B97,^{122,123} and PBE0,^{85,124} typically use approximately 20–25% exact exchange. Hybrids designed to reduce delocalization error for chemical kinetics, such as MPW1K¹²⁵ and M06-2X,¹²⁶ use larger fractions, near 50% exact exchange.

Building on global hybrid functionals are range-separated hybrids,^{127–136} where the degree of exact-exchange mixing is dependent on the interelectron distance (r_{12}). This is achieved by separating the exchange terms into short-range and long-range components via an error function,

$$\frac{1}{r_{12}} = \underbrace{\frac{1 - \text{erf}(\omega r_{12})}{r_{12}}}_{\text{short range}} + \underbrace{\frac{\text{erf}(\omega r_{12})}{r_{12}}}_{\text{long range}}, \quad (7)$$

where ω is the range-separation parameter. The exchange-correlation energy is evaluated for the two components separately, using different methods, and the results then recombined. In periodic systems, functionals with full GGA exchange at long range, such as HSE,^{135,136} are used to reduce the computational cost associated with hybrid DFT. In molecular systems, functionals with full HF exchange at long range, such as LC-BLYP,¹²⁹ LC- ω PBE,^{132,133} and ω B97X,¹³⁴ are used to minimize delocalization error. While there are additional classes of functionals that depend on the exact exchange-energy density, or the unoccupied (virtual) KS orbitals, these will not be discussed until Section 5.

2.2 | Self-interaction error

Self-interaction arises from the Coulomb energy terms that correspond to interaction of an electron with itself. For a one-electron system, the Coulomb energy given by Equation (5) is nonzero, which is not physical. However, in Hartree–Fock theory, the nonzero Coulomb energy for interaction of an electron with itself is offset by a corresponding exchange-energy term that is equal in magnitude, but opposite in sign. The exact (Hartree–Fock) exchange energy is

$$E_X = \frac{1}{2} \sum_{\sigma} \int \int \frac{1}{r_{12}} \psi_{i\sigma}(\mathbf{r}_1) \psi_{j\sigma}(\mathbf{r}_2) \psi_{j\sigma}(\mathbf{r}_1) \psi_{i\sigma}(\mathbf{r}_2) d\mathbf{r}_1 d\mathbf{r}_2, \quad (8)$$

where σ indicates electron spin and the ψ 's are the occupied KS orbitals, assumed to be real. Thus, the HF exchange energy is also nonzero for a single electron.

For a one-electron system with a single occupied orbital, the requirement for vanishing self-interaction energy is⁶³

$$J_{ee} + E_X = 0. \quad (9)$$

This condition is satisfied by the exact (HF) exchange energy due to the offsetting Coulomb and exchange integrals. However, for DFAs, such as the LSDA or GGAs, the exchange energy does not offset the self-Coulomb energy. Indeed, the DFA exchange energy can be much larger in magnitude than the exact exchange energy in some systems, resulting in overstabilization.

The classic example of this is the dissociation limit of the H_2^+ potential energy curve, which is described exactly by HF theory. However, this dissociation limit is predicted to be far too low in energy by most DFAs,^{4,25,26,28} as shown in Figure 1a for the LSDA,⁶³ and for BLYP^{83,120} and PBE,⁸⁵ which are representative GGA functionals. Results are also shown for two meta-GGAs: M06L¹⁰² and SCAN.¹⁰⁵ The dissociation limit obtained with each DFA is far below the exact result from HF theory. Figure 1b shows analogous results for He_2^+ . Here, HF is not exact since He_2^+ is not a one-electron system and, due to neglect of electron correlation effects, it gives a dissociation limit above the CCSD(T) reference. All the DFAs again fail catastrophically, predicting He_2^+ with a highly stretched bond length to be far lower in energy than the separated He atom and He^+ ion. These results are not unique to the specific functionals chosen; all GGAs and meta-GGAs show similar errors.²⁸

SIE can be reduced through use of hybrid functionals, since they include some fraction of exact exchange. However the optimum exchange-mixing fraction is clearly system dependent. For a uniform electron gas, the LSDA is exact and there is no SIE. Bulk metals are the systems that most closely resemble a uniform electron gas, and are typically very well treated by the LSDA and GGA functionals. Conversely, for one-electron systems, full exact exchange is needed to eliminate SIE. Most many-electron systems fall somewhere between these two extremes, where some optimal mixing of DFA and HF exchange will minimize SIE. As a result, SIE is identified in practice in cases where the LSDA or GGAs drastically over-stabilize a particular system and the error decreases with increasing exact-exchange mixing, usually up to approximately 50% HF exchange for a global hybrid or 100% long-range HF exchange for a range-separated hybrid.

2.3 | Self-interaction corrections

To improve performance of the LSDA (or GGAs), Perdew and Zunger⁶³ developed a one-electron self-interaction correction (SIC). This correction uses single-orbital spin densities,

$$\rho_{i\sigma}(\mathbf{r}) = \psi_{i\sigma}^2, \quad (10)$$

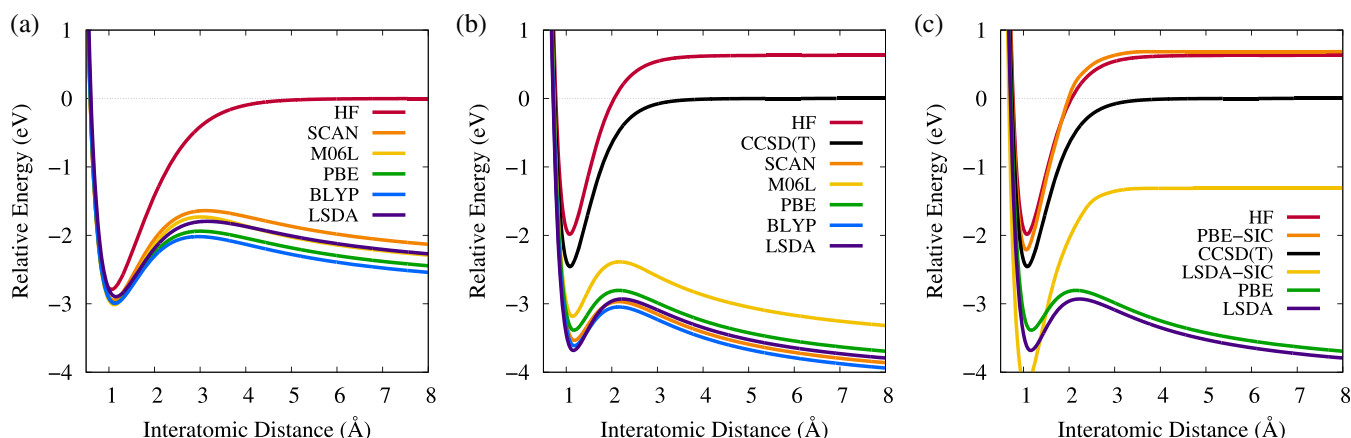


FIGURE 1 Potential energy curves for (a) H_2^+ and (b) He_2^+ obtained with selected methods and the aug-cc-pVTZ basis set using Gaussian 16¹³⁷ (psi4¹³⁸ for the SCAN calculations). Also shown in (c) are LSDA and PBE potential energy curves for He_2^+ with the Perdew-Zunger self-interaction correction⁶³ (SIC) obtained using the PyFLOSIC code.¹³⁹

such that the total density is a sum of all the one-electron spin densities. The self-interaction-corrected exchange-correlation energy is then

$$E_{XC}^{\text{SIC}} = E_{XC}(\rho_\alpha, \rho_\beta) - \sum_{i\sigma} [J_{ee}(\rho_{i\sigma}) - E_{XC}(\rho_{i\sigma})], \quad (11)$$

where ρ_α and ρ_β are the α - and β -spin indexed electron densities. The term in square brackets resembles the left-hand side of Equation (9) and is the SIC for orbital i with spin σ . This term would be identically zero for either HF or the exact exchange-correlation functional. An analogous SIC can be formulated for the exchange-correlation potential, which allows solution for a set of corrected KS orbitals and energy eigenvalues.⁶³ The correction to the eigenvalues allows the SIC method to improve DFA predictions of band gaps.^{140–144}

For the H_2^+ example, any SIC-corrected functional will necessarily give the exact (Hartree–Fock) result since Equation (11) is designed to recover the HF energy for one-electron systems. However, Equation (11) provides only an approximate correction for many-electron systems. As shown in Figure 1c, the SIC corrects the shape of the He_2^+ PES when applied to both PBE and the LSDA, although it does not recover the exact dissociation limit corresponding to the sum of the separated He and He^+ energies.

Unfortunately, the SIC tends to worsen predicted properties of molecules exhibiting minimal SIE,^{145–149} so a scaled SIC of the form

$$E_{XC}^{\text{SIC}} = E_{XC}(\rho_\alpha, \rho_\beta) - \sum_{i\sigma} X_{i\sigma} [J_{ee}(\rho_{i\sigma}) - E_{XC}(\rho_{i\sigma})], \quad (12)$$

was introduced.¹⁵⁰ Here, $X_{i\sigma}$ is a scaling factor,

$$X_{i\sigma} = \int z_\sigma^k \rho_{i\sigma}(\mathbf{r}) d\mathbf{r}, \quad (13)$$

with

$$z_\sigma = \frac{\tau_\sigma^W(\mathbf{r})}{\tau_\sigma(\mathbf{r})}, \quad (14)$$

such that $0 < X_{i\sigma} \leq 1$. $\tau_\sigma = \frac{1}{2} \sum_i |\nabla \psi_{i\sigma}|^2$ is the σ -spin kinetic-energy density, τ_σ^W is the von Weizsäcker kinetic-energy density,

$$\tau_\sigma^W(\mathbf{r}) = \frac{|\nabla \rho_\sigma(\mathbf{r})|^2}{8\rho_\sigma(\mathbf{r})}, \quad (15)$$

and $k \geq 0$ is a scaling exponent. This form recovers the original PW SIC for $k = 0$ and the uncorrected DFA result in the limit of $k \rightarrow \infty$.¹⁵⁰ In practice, k values of 1 or 2 were chosen to provide improved performance for molecular properties.^{150,151}

This scaling does not affect the H_2^+ PES as $\tau = \tau^W$ for all one-electron systems. The scaling also has only a minor effect on the computed PES for He_2^+ .¹⁵¹ However, it was found that reduction of the SIC through this scaling substantially degrades performance for the PES of Ne_2^+ ¹⁵¹ and for NaCl.⁶⁶ In the latter case, the LSDA and GGAs predict a dissociation limit with spurious fractional charges on both atoms. Ultimately, this leads to a similar situation seen with the amount of exact-exchange mixing in hybrid functionals, where no single choice of %HF or k works well for all systems. Optimizing k for thermochemistry still results in significant SIE, while taking $k = 0$ to minimize SIE worsens molecular properties, hampering the general applicability of SICs. One solution is to introduce a local, position-dependent scaling.^{152–154} In the resulting local self-interaction correction (LSIC) scheme, the corrected exchange-correlation energy is analogous to Equation (11), but with the J_{ee} term replaced by

$$U^{\text{LSIC}}(\rho_{i\sigma}) = \frac{1}{2} \int \int f[z_\sigma(\mathbf{r}_1)] \frac{1}{r_{12}} \rho_{i\sigma}(\mathbf{r}_1) \rho_{i\sigma}(\mathbf{r}_2) d\mathbf{r}_1 d\mathbf{r}_2, \quad (16)$$

and the E_{XC} term replaced by

$$E_{\text{XC}}^{\text{LSIC}}(\rho_{i\sigma}) = \int f[z_\sigma(\mathbf{r})] \varepsilon_{\text{XC}}[\rho_{i\sigma}(\mathbf{r})] d\mathbf{r}, \quad (17)$$

where ε_{XC} is the exchange-correlation energy density. $f(z_\sigma)$ is some function with values between 0 and 1, with the simplest alternative being z_σ^k . It can also be shown that this local scaling can be written as a global scaling after a change of gauge.¹⁵⁵

A key drawback of the SIC is that it is orbital dependent and, hence, is not invariant with respect to unitary orbital transformations. This means that the value of the SIC will depend on the choice of orbitals. Using the KS orbitals is intuitive, but their highly nonlocal nature means that the SIC will approach zero in the bulk limit.^{63,156} This can be resolved by using localized orbitals, but there are many possible localization schemes and the magnitude of the SIC will depend on the particular one selected. Recent development work has focused on Fermi-Löwdin orbitals (FLO),^{139,156–158} which provide a convenient framework for general application of the SIC to chemical systems of any size.^{159–163} Ongoing development has involved orbital-dependent scaling,^{150,164} as well as use of FLOSIC with the density-consistent effective potential^{165,166} or the Krieger-Li-Iafrate^{167,168} approximation to the optimized effective potential.

2.4 | The fractional-charge picture

An alternative, but complementary, view of SIE considers gradual ionization of ensembles of atoms or molecules. Removal (or addition) of one electron from an ensemble of symmetry-equivalent atoms will result in a fractional charge on each atom in the ensemble.^{64,67,114,169,170} Assuming the atoms are sufficiently far apart to be noninteracting, then the energy should be equivalent to that of an isolated ion and many neutral atoms. For our stretched H_2^+ example, each H atom will have a fractional charge of +0.5 and the energy should be equal to that of the separated H atom and H^+ ion, which is the correct dissociation limit. We can extend the number of atoms, n , in the ensemble and remove the appropriate number of electrons, $p < n$, to obtain any fractional charge, $q = \frac{p}{n}$, on each H atom, giving $(\text{H}^{+q})_n$. The energy of such an ensemble should then be equal to the sum of the energies of $(n - p)$ H atoms and $p \text{ H}^+$ ions. Similarly, if we add $p < n$ electrons, the fractional charge would be $q = -\frac{p}{n}$, resulting in an ensemble energy equal to $(n - p)$ H atoms and $p \text{ H}^-$ ions. More generally, it can be proven that the total energy for any atom should be piecewise linear in fractional charge, q , with derivative discontinuities occurring at the integer values.⁶⁴

In practice, fractional-charge calculations cannot be performed by most electronic-structure codes. However, such curves can be drawn by using a cubic spline of the form.^{171,172}

$$E(x) = E_{N-1} + \Delta E(x + 1 - N) + (N - x)(x + 1 - N) [(e_{N-1}^{\text{LUMO}} - \Delta E)(N - x) + (\Delta E - e_N^{\text{HOMO}})(x + 1 - N)], \quad (18)$$

where x is the total number of electrons, such that $N - 1 \leq x \leq N$, and $\Delta E = E_N - E_{N-1}$. The energies of the integer-charged species (E_N and E_{N-1}) are computed by conventional electronic-structure calculations. The slope at $x = N - 1$ is the LUMO (lowest unoccupied molecular orbital) eigenvalue of the $(N - 1)$ -electron species, e_N^{LUMO} , while the slope at $x = N$ is the HOMO (highest occupied molecular orbital) eigenvalue of the N -electron species, e_N^{HOMO} , in accordance with Janak's theorem.¹⁷³

As an illustration, we show the energy of the Li atom as a function of varying number of electrons from Li^+ ($x = 2$) to Li^- ($x = 4$) in Figure 2 for several selected DFAs. Also shown is the deviation from the ideal, linear behavior, obtained by omitting the first two terms from the right-hand side of Equation (18). The largest deviations from linearity are seen for the GGA functional (PBE), which gives concave-up curves and over-stabilizes the fractionally charged species. The excess stabilization of $\text{Li}^{+0.5}$ implies that the dissociation limit of Li_2^+ will also be too low in energy, similar to what was seen in Figure 1 for H_2^+ and He_2^+ .

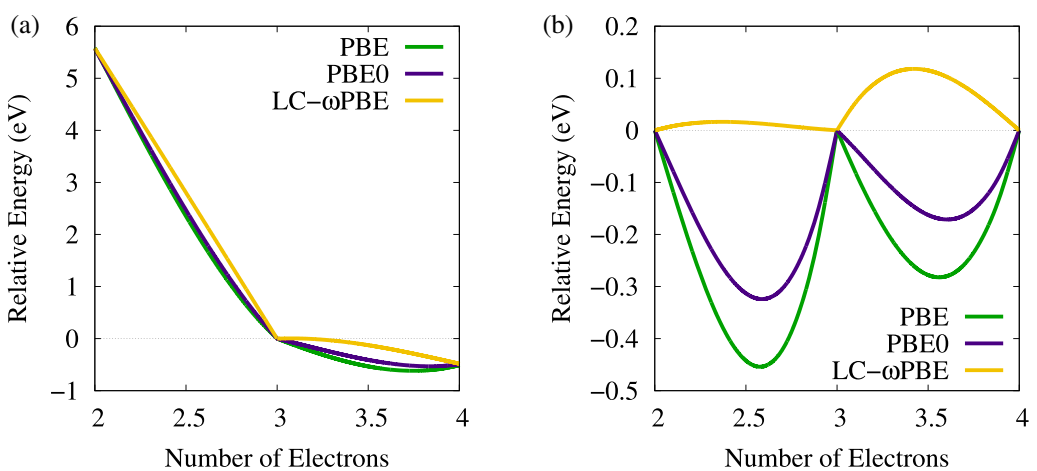


FIGURE 2 Relative energies for Li as a function of electron number: (a) total energies and (b) deviation from ideal, linear behavior. Calculations were performed using Gaussian 16 and the aug-cc-pVTZ basis set.¹³⁷

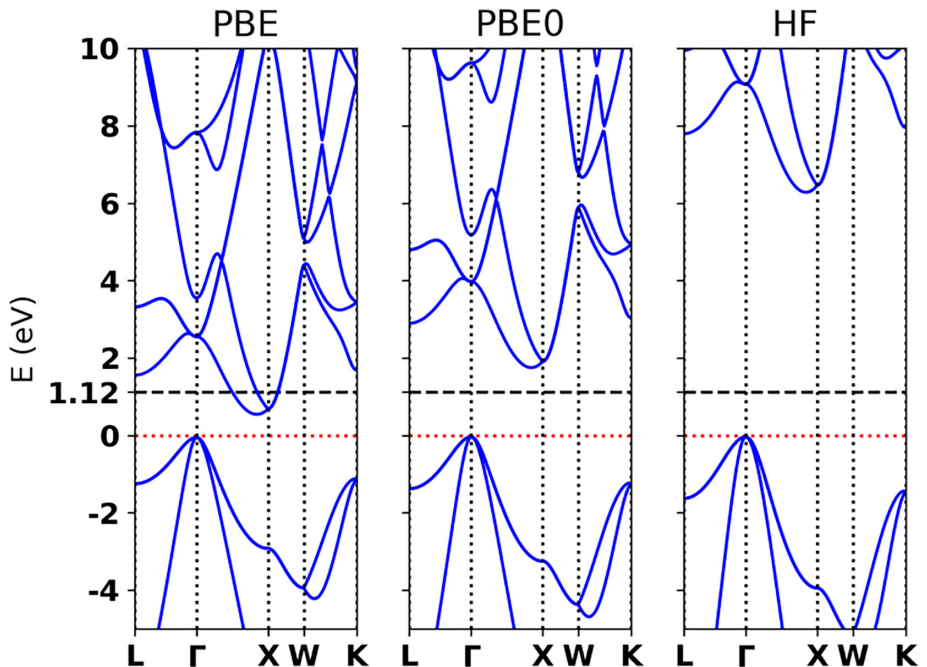


FIGURE 3 Dependence of the computed band structure of bulk silicon on the extent of exact-exchange mixing. Calculations were performed using the all-electron code FHI-aims.¹⁷⁴ All calculations use numerical atom-centered orbital basis sets with the FHI-aims “light” settings and a $12 \times 12 \times 12$ k-space grid. A lattice constant of 5.416 \AA was used. The zero of energy is taken as the top of the valence band in all cases and the experimental band gap of 1.12 eV ¹⁷⁵ is shown for comparison.

The fractional-charge interpretation of delocalization error is particularly convenient to explain the band-gap problem.^{41,42} This problem refers to the tendency of many DFAs, particularly the LSDA and GGAs, to underestimate the band gaps of semi-conductors,^{39,40} as illustrated in Figure 3 for bulk silicon. The molecular equivalent of the band gap is the HOMO-LUMO gap, which is the difference between the HOMO and LUMO eigenvalues. The orbital eigenvalues are the derivatives of the energy with respect to electron number,¹⁷³

$$\epsilon^{\text{HOMO}} = \lim_{x \rightarrow N^-} \frac{E(x) - E(N)}{x - N}, \quad (19)$$

$$\varepsilon^{\text{LUMO}} = \lim_{x \rightarrow N+} \frac{E(x) - E(N)}{x - N}, \quad (20)$$

such that the HOMO energy is the derivative from below, the LUMO energy is the derivative from above, and there is a derivative discontinuity at the integer points.⁶⁴ Since plots of the LSDA and GGAs energies with respect to fractional charges are concave up, the HOMO is too high in energy (i.e. the slope is not steep enough) and the LUMO is too low in energy (i.e. the slope is too steep), as illustrated in Figure 4. This results in closing of the HOMO-LUMO gap in a finite molecular system with GGAs and, hence, the band gap in a bulk solid.

Returning to Figure 2, the deviations from linearity seen with the PBE GGA are reduced by inclusion of some fraction of exact (Hartree-Fock) exchange, as in PBE0 (25% HF exchange). Including large fractions of exact exchange, as in LC- ω PBE (100% HF exchange for large r_{12}), can reverse the sign of the error and give concave-down curves, under-stabilizing the fractionally charged species. This can be referred to as a “localization” error, in contrast to delocalization error. Localization errors seen with HF theory itself stem from neglect of electron correlation rather than an inexact form of the exchange functional. This neglect of correlation results in HF's vast overestimation of the band gap seen in Figure 3, and a similar localization error is seen with HF for the dissociation limit of He_2^+ in Figure 1. MP2 and other correlated wavefunction theories are effectively free of delocalization or localization error and their energies vary (nearly) linearly with fractional charge.¹⁷⁶ In range-separated hybrid functionals, long-range, nonlocal correlation is required to be compatible with the full long-range exact exchange, and its absence leads to a localization error, similar to that seen with HF.

HF theory and some density functionals designed to reduce delocalization error^{63,177–179} give energies that vary linearly with fractional charge for one-electron systems by construction. However, such methods display nonlinear behavior for many-electron systems and hence still have inherent errors^{65,66,151,180} that affect predictions of thermochemistry, reaction barrier heights, band gaps, polarizabilities, charge transfer, and other properties. This lead to the distinction between one-electron and many-electron SIE,^{65,66,151,180} while delocalization error is often used as a more general, aggregate term. A DFA is defined to be “ N -electron self-interaction free” if the energy varies linearly with fractional electron number, x , such that

$$E(x) = E_{N-1}(N-x) + E_N(x+1-N), \quad (21)$$

for $N-1 \leq x \leq N$. Functionals that are free of 1-electron SIE will give the correct dissociation limit for H_2^+ and tend to perform well for H-atom transfer barriers.^{35,36,177,181,182} However, functionals capable of correcting for many-electron SIE (i.e. for some general $N \geq 2$) are required more frequently and this remains an open area for functional development.

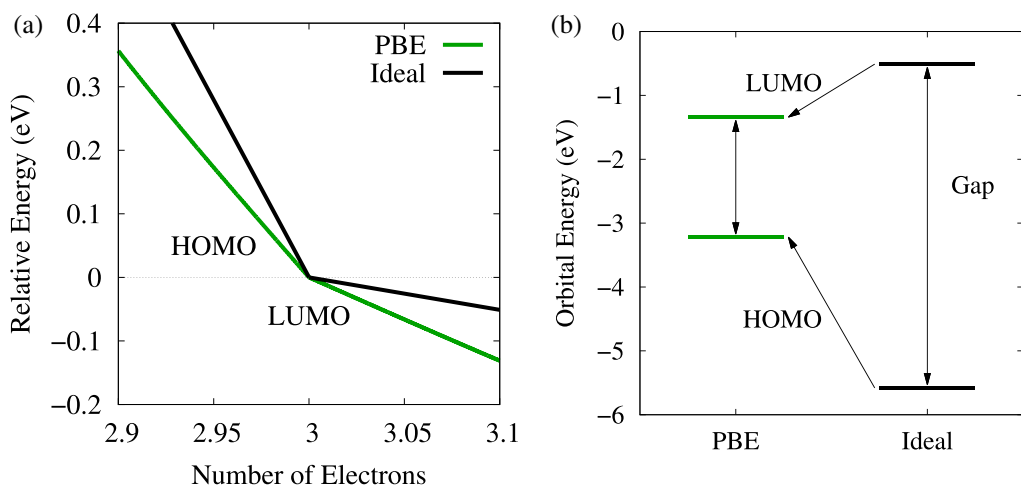


FIGURE 4 Illustration of how fractional-charge errors with common density-functional approximations lead to band-gap closing, for the example of the Li atom.

Piecewise linearity of the total energies is now a common test to assess the performance of new functionals. Notably, range-separated hybrids are typically capable of satisfying Equation (21) for a given molecule with a certain choice of the range-separation parameter (ω in Equation 7). System-specific ω -tuning, such as to enforce Koopmans' theorem that the ionization potential equal the HOMO eigenvalue, can be used to obtain improved excitation energies and other properties.^{183–195} However, as the particular ω value required to minimize N -electron SIE is system dependent,^{172,184,196–198} the piecewise-linear energy constraint cannot be satisfied simultaneously for a diverse set of molecules. The recent localized orbital scaling correction (LOSC)^{199–203} was developed to enforce the piecewise-linearity constraint and shows good performance for many common systems that showcase delocalization error.

2.5 | The exchange-correlation hole picture

A final way to understand SIE is through visualization of the exchange-correlation hole.^{4,204,205} Given an electron at a fixed reference point, the hole measures the depletion in probability of finding a second electron a certain distance away from that point. HF theory gives an exchange hole that is delocalized over all atoms in a system, but correlation usually serves to localize the full exchange-correlation hole to within regions of roughly atomic size.^{4,206} Conversely, most DFAs, and particularly the LSDA and GGAs, already model exchange holes as being fairly localized about each reference point.^{76,84,96} This is typically advantageous as the model holes implicitly build in nondynamical correlation effects. However, in situations with significant SIE, nondynamical correlation is insufficient to localize the hole and the exact exchange-correlation hole remains delocalized, in a similar way to the HF hole. In such cases, the assumptions made in construction of model DFA exchange holes are no longer valid.

As an example, we contrast the hydrogen atom, where DFAs give effectively zero SIE, with the H_2^+ dissociation limit. From the discussion in Section 2.4, the dissociation limit of H_2^+ is equivalent to two $H^{+0.5}$ cations. For simplicity, the electron density of $H^{+0.5}$ is approximated as half the H-atom density. Figure 5a,d illustrates these two density distributions.

Since there is no electron correlation in either H or $H^{+0.5}$, we can focus entirely on the exchange hole. We use the Becke–Roussel⁹⁶ (BR) meta-GGA for this demonstration since it is conveniently based on a real-space representation of the exchange hole as a simple exponential function displaced from the reference point. It is also constrained to recover the density and curvature of the exact exchange hole at the reference point. The DFT exchange energy is uniquely determined by the exchange hole via

$$E_X = \frac{1}{2} \sum_{\sigma} \int \int \frac{\rho_{\sigma}(\mathbf{r}_1)}{r_{12}} h_{X\sigma}(\mathbf{r}_1, \mathbf{r}_2) d\mathbf{r}_1 d\mathbf{r}_2. \quad (22)$$

It can also be shown that the exchange energy is dependent only on the spherical average of the hole about the reference point:²⁰⁷

$$E_X = 2\pi \sum_{\sigma} \int \int \frac{\rho_{\sigma}(\mathbf{r})}{s} h_{X\sigma}(\mathbf{r}, s) s^2 ds d\mathbf{r}. \quad (23)$$

The normalization of the spherically averaged hole is

$$N = 2\pi \sum_{\sigma} \int \int h_{X\sigma}(\mathbf{r}, s) s^2 ds d\mathbf{r}, \quad (24)$$

which is typically constrained to -1 electron in construction of DFAs.

Figure 5b,e shows the negative integrand of the hole normalization (Equation 24) for the spherical average of the exact and BR exchange holes for two choices of reference point, \mathbf{r} , in H and $H^{+0.5}$. For the H atom, both the exact and DFA holes are normalized to -1 electron, and the BR hole model is exact by construction, so both curves are overlaid. Conversely, for $H^{+0.5}$, the normalization integrand for the BR hole is larger in magnitude than that of the exact hole

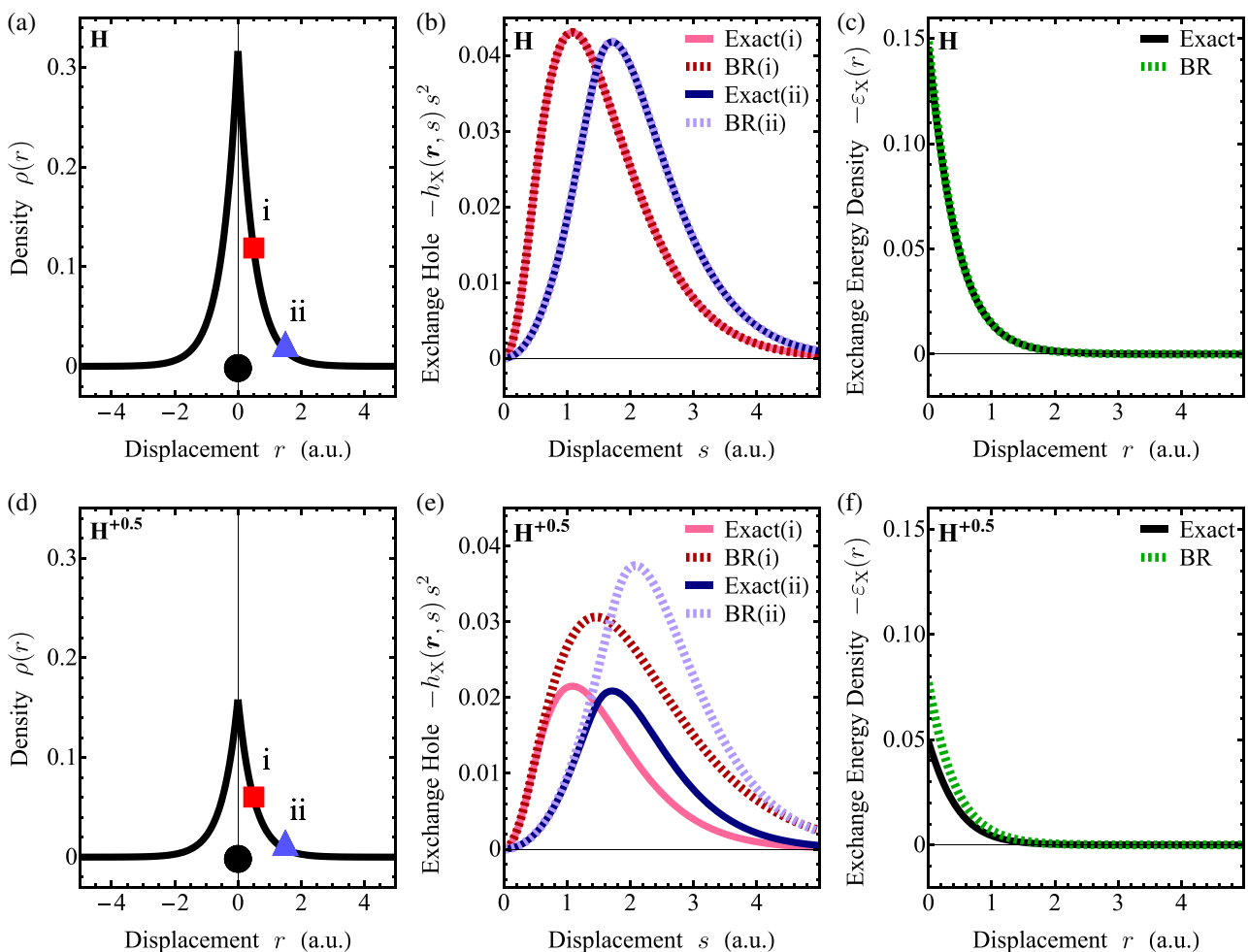


FIGURE 5 Plots of the total electron density (a,d) and the normalization integrand for spherical averages of BR and exact exchange holes (b,e) about the two shown reference points for H (top row) and $H^{+0.5}$ (bottom row). Also shown are the exchange-energy densities for both species (c,f). All quantities are given in Hartree atomic units (a.u.).

away from the reference point. This occurs because DFA holes, including the BR holes shown in Figure 5, are always assumed to have unit normalization. However, the exact exchange hole in $H^{+0.5}$ is only normalized to $\frac{-1}{2}$ an electron due to the fractional charge.

Since the exchange energy is determined by the exchange hole via Equation (23), having double the normalization from the DFA model hole results in effectively double counting the exchange energy. To illustrate this more clearly, we also plot the exchange-energy density,

$$\varepsilon_X(\mathbf{r}) = 2\pi\rho_\sigma(\mathbf{r}) \int h_{X\sigma}(\mathbf{r}, s) s ds, \quad (25)$$

such that the exchange energy is

$$E_X = \sum_\sigma \int \varepsilon_X(\mathbf{r}) d\mathbf{r}. \quad (26)$$

Results are shown for both H and $H^{+0.5}$ in Figure 5c,f. The BR functional recovers the exact exchange-energy density for H, but gives an exchange-energy density that is too large in magnitude for $H^{+0.5}$, most noticeably near the nucleus. This results in a large total energy error and explains the behavior seen for the various DFAs for the H_2^+ PES

in Figure 1a. At equilibrium, the exact exchange hole will have near unit normalization and DFAs provide quite accurate energies. However, as the dissociation limit is approached, the exact hole normalization will approach $\frac{-1}{2}$ about each nucleus and DFAs will overestimate the magnitude of the exchange contribution to the total energy. An analogous argument can be made for He_2^+ and other stretched odd-electron systems as well.^{4,25–28,208}

Thus, we conclude that delocalization error occurs when the model DFA exchange-correlation hole has a normalization that is too large relative to the exact exchange-correlation hole. This view is consistent with the previous discussion of SIE in Section 2.2, as the Perdew–Zunger SIC can be recast in terms of the exchange hole and serves to reduce the hole normalization.^{63,151}

3 | ENERGY- VERSUS DENSITY-DRIVEN ERRORS

3.1 | Classification of errors

For all of the examples discussed so far, the electron densities predicted by DFAs are qualitatively correct, and the SIE or delocalization error arises from the DFA energy. However, there are other examples where the DFA electron density itself is qualitatively incorrect, exhibiting an excess delocalization of charge. In such cases, the DFA electron density can be significantly different than what would be expected from correlated wavefunction theory, or even chemical intuition. One such example occurs for the Cl^- anion surrounded by six water molecules to represent the first solvation shell.^{67,200} Here, we would expect the excess charge to remain localized on the Cl atom, but GGA calculations instead delocalize the charge. Figure 6 shows density difference maps for $\text{Cl}^- \cdot (\text{H}_2\text{O})_6$ versus $\text{Cl} \cdot (\text{H}_2\text{O})_6$ to visualize the spatial distribution of the excess charge. This illustrates why many-electron SIE is commonly termed delocalization error. Another dramatic example of qualitatively incorrect density distributions from GGAs occurs for solvated-electron model systems.¹⁷¹ In this case, functionals with delocalization error incorrectly preferred fractional charges and, as the degree of delocalization error increased, unpaired electrons were shared nearly equally between distant moieties.

Sim, Burke, and co-workers coined the terms “energy-driven” and “density-driven” delocalization errors to differentiate between its two manifestations.²⁰⁹ To quantitatively distinguish between these two classes of errors, we compare the results from the usual self-consistent DFT calculations (SCF) with those from density-corrected DFT,^{210–217} in which DFA energies are calculated in a post-SCF fashion using the converged HF orbitals and electron density. The SCF calculations will include both energy- and density-driven errors, while the post-HF calculations will only involve energy-driven errors since the HF densities are free of delocalization error by construction. If using the HF densities significantly reduces or eliminates the delocalization error, then it must be density driven. Conversely, if the SCF and post-HF calculations give similar results, then the delocalization error is energy driven.

To illustrate this analysis, Table 1 compares mean absolute errors (MAEs) and mean errors (MEs) for four benchmark sets obtained using both SCF and post-HF calculations. Results are shown for four functionals with varying extents of exact-exchange mixing: the PBE⁸⁵ GGA (0% HF), the SCAN¹⁰⁵ meta-GGA (0% HF), the PBE0¹²⁴ hybrid (25% HF), and the LC- ω PBE^{132,133} range-separated hybrid (100% HF at large r_{12}). In most cases, the MAEs decrease in the

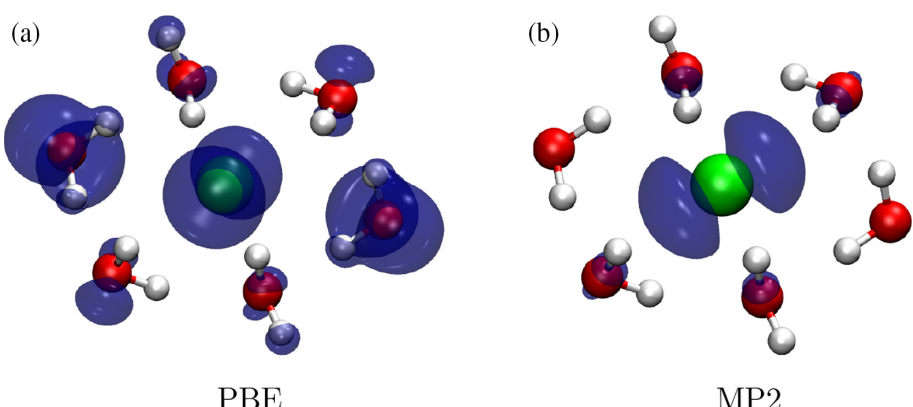


FIGURE 6 Density difference maps for $\text{Cl}^- \cdot (\text{H}_2\text{O})_6$ relative to $\text{Cl} \cdot (\text{H}_2\text{O})_6$ using PBE (0.002 a.u. isosurface) and MP2 (0.006 a.u. isosurface). Calculations were performed with the 6-31+G* basis set using the Gaussian program.¹³⁷

order PBE > SCAN > PBE0 > LC- ω PBE, as expected, since SCAN has more inherent SIC than PBE and increased exact-exchange mixing reduces delocalization errors.

3.2 | Energy-driven errors

The dissociation limits of the simple ions shown in Figure 1 are all examples of energy-driven errors since the DFA density distributions are essentially correct, with the charge split evenly between the two fragments due to symmetry. To encapsulate these into a simple benchmark, Goerigk, Grimme, and co-workers created the SIE4 \times 4 set,¹⁰⁹ which consists of four geometries for each of H₂⁺, He₂⁺, (NH₃)₂⁺, and (H₂O)₂⁺. The high-level reference binding energies, relative to the separated neutral and cation species, were obtained from W4 theory.²²⁰ The SIE4 \times 4 MAEs in Table 1 decrease only marginally using post-HF densities, confirming energy-driven delocalization error.

Energy-driven errors also occur for systems with extended conjugation, where GGAs overstabilize the delocalized electron density in the π system. In the solid state, this results in overstabilization of graphite relative to diamond,⁵⁵ while in molecular calculations it can affect the energy ordering of C₂₀ isomers,⁵⁴ although both of these examples are complicated by the role of London dispersion. A simpler benchmark can be assembled from the work of Woodcock and co-workers on the relative stabilities of cumulenes and poly-ynes.⁵⁰ For the cumulenes (allene, penta-1,2,3,4-tetraene, and hepta-1,2,3,4,5,6-hexaene), the alternating π -bonds lie in orthogonal planes from each other, inhibiting conjugation. Conversely, for the poly-ynes (propyne, penta-1,3-diyne, and hepta-1,3,5-triyne), the alternating single and triple bonds allow extended conjugation along the full length of each molecule. As a result, GGAs overstabilize the poly-ynes relative to the cumulenes when compared to high-level CCSD(T) reference data.⁵⁰ The DFA MAEs for this isomerization benchmark in Table 1 again show only small decreases using HF densities, which is indicative of an energy-driven error.

3.3 | Density-driven errors

Underestimation of barrier heights for simple H-atom transfer reactions, such as the H + H₂ identity reaction, is a well-known example of delocalization error.^{33–35} The finding that large amounts of HF exchange mixing, near 50%, yielded improved performance lead to development of hybrid functionals targeted for chemical kinetics.^{125,126} Lynch and Truhlar's BH22 set³³ of (forward and reverse) barrier heights for 22 H-atom transfer reactions is the established benchmark. It has also been known for some time that using HF densities for DFA energy evaluation (i.e. density-corrected DFT) improves accuracy for these barriers.³⁸ A comparison of the SCF and post-HF results for the BH22 set with selected functionals is shown in Table 1 and confirms this to be a case of primarily density-driven delocalization error. This is likely because the GGA and meta-GGA functionals do not sufficiently localize the unpaired electron within the transition-state structure.

TABLE 1 Mean absolute errors (in kcal/mol) for four delocalization-error benchmarks obtained with four selected density-functional approximations (DFAs). Results use either self-consistent DFA orbitals (SCF) or converged HF orbitals (HF). Mean errors are shown in parentheses, with negative values indicating overbinding. All calculations were performed using the aug-cc-pVTZ basis set (except for the XB benchmark, which used aug-cc-pVQZ) and Grimme's D3(BJ) dispersion correction²¹⁸ with Gaussian¹³⁷ (psi4¹³⁸ for the SCAN calculations).

Functional	Density	SIE4 \times 4 ¹⁰⁹		Isomers ⁵⁰		BH22 ³³		XB ^{59,219}	
PBE	SCF	23.5	(−23.5)	9.8	(−9.8)	10.2	(−10.2)	3.15	(−3.15)
	HF	18.3	(−18.3)	7.3	(−7.3)	3.6	(−3.3)	0.77	(−0.47)
SCAN	SCF	17.9	(−17.9)	8.5	(−8.5)	7.8	(−7.8)	3.41	(−3.39)
	HF	14.1	(−14.1)	6.3	(−6.3)	3.5	(−3.3)	1.42	(−1.15)
PBE0	SCF	14.3	(−14.3)	6.6	(−6.6)	5.1	(−5.1)	2.36	(−2.36)
	HF	11.1	(−11.1)	5.1	(−5.1)	1.7	(−1.1)	0.97	(−0.86)
LC- ω PBE	SCF	9.6	(−9.6)	0.9	(−0.9)	1.5	(−1.0)	0.74	(0.16)
	HF	6.9	(−6.5)	0.3	(−0.2)	2.2	(2.0)	0.64	(0.50)

The second example of density-driven delocalization error in Table 1 is Bauza's set of halogen-bonded (XB) complexes,²¹⁹ with updated reference data.⁵⁹ Halogen bonding refers to a favorable noncovalent interaction between the negatively charged lone pair of one atom (a pnictogen, chalcogen, or halogen) and the positively charged σ -hole of a halogen.^{221–224} Analogous interactions can also form involving σ -holes of chalcogen atoms and are termed chalcogen bonding.^{225–227} Both halogen- and chalcogen-bonded complexes tend to exhibit substantial charge transfer and, consequently, are susceptible to density-driven delocalization error.^{59–61} Such errors are magnified in the Bauza set, relative to other halogen-bonding benchmarks,^{228,229} since it contains many complexes involving Cl^- or Br^- anions. As shown in Table 1, use of the HF densities significantly lowers the MAEs obtained with PBE, SCAN, and PBE0, confirming that the errors for this benchmark are density driven.

The BH22 and XB results illustrate the utility of density-corrected DFT,^{210–215} where DFA energies are evaluated in a post-HF fashion in production calculations to eliminate density-driven delocalization error. Density-corrected DFT can also improve performance for many additional benchmarks within the GMTKN55 set²¹⁶ and notably results in excellent performance of the SCAN functional for water.²¹⁷ However, this approach can neither correct for energy-driven errors, nor can it be applied to cases where delocalization error affects predicted structures, unless gradients are implemented for geometry optimization. Additionally, the use of a HF density will not always improve DFA results, particularly for conjugated radicals and some transition-metal compounds, where HF can suffer from severe spin contamination.²³⁰

3.4 | Effects of delocalization error on geometries

In some cases, delocalization error in the energy or density is sufficient to significantly alter molecular geometries. Simple molecular systems where delocalization error alters the potential energy surface and leads to qualitatively incorrect geometries are the $\text{HO}\cdot\text{Cl}^-$ radical anion²¹⁰ and several transition-metal triatomics.²³¹ Two further examples are shown in Table 2. First is the pre-reaction complex for hydrogen-atom transfer between 1,4-diazabicyclo[2.2.2]octane (DABCO) and the benzyloxy radical.²³² With GGA functionals, there is considerable charge transfer in this complex. The C–H bond of the benzyloxy radical (nearly perpendicular to the plane of the aromatic ring) becomes stretched and the N–H intermolecular contact compressed, forming a strong C–H–N pseudo hydrogen bond. The second example is the intermediate of the thio-Michael addition reaction of methylthiolate anion to methylvinylketone.^{233,234} While this reaction should proceed via an enolate intermediate, GGA functionals instead optimize the structure to that of a charge-transfer complex without a formal C–S bond. In both cases, the binding energies show the clear trend of decreasing with increased exact-exchange mixing, as is characteristic of delocalization error. Further, the extent of charge transfer between the interacting fragments also decreases sharply with increased exact-exchange mixing, indicating the error to be density driven.

TABLE 2 Illustration of density-driven delocalization error on molecular geometry for the benzyloxy-DABCO pre-reaction complex²³² (top) and the enolate intermediate for thio-Michael addition^{233,234} (bottom). Key interatomic distances (R in Å), binding energies relative to the separated molecules (ΔE in kcal/mol), and extent of Mulliken charge transfer (CT in e^-), are shown for three selected density-functional approximations. The DFT calculations were performed using the 6–31+G* basis set and Grimme's D3(BJ) dispersion correction²¹⁸ with the Gaussian program.¹³⁷

Method	R(C–H)	ΔE	CT
PBE	1.179	15.2	0.166
PBE0	1.169	10.1	0.092
LC- ω PBE	1.129	8.2	0.008

Method	R(C–S)	ΔE	CT
PBE	2.187	26.0	0.270
PBE0	1.966	23.5	0.124
LC- ω PBE	1.878	21.9	0.060

Even more dramatically, delocalization error can result in changes in protonation state in organic acid–base co-crystals.⁶² Here, geometry relaxation can result in spontaneous proton transfer from the acid to the base, incorrectly predicting neutral co-crystals to exist as organic salts. Examples such as these are particularly challenging tests for methods designed to reduce delocalization error, as they require corrections not just to the density or energy, but also to the energy gradients required for geometry optimization.

4 | CONNECTION WITH DISPERSION CORRECTIONS

4.1 | DFA descriptions of nonbonded repulsion

The characteristic signature of delocalization error is improved performance with increased exact-exchange mixing. However, care must be taken to be sure that such situations are in fact caused by SIE and not another systematic error in DFAs. One competing error that can be mistaken for SIE lies in the treatment of nonbonded repulsion, which is controlled by the form of the enhancement factor in most DFA exchange functionals.^{87–95} All GGA functionals share the general form

$$E_X^{\text{GGA}} = \sum_{\sigma} \int \varepsilon_{X,\sigma}^{\text{LSDA}} F(\chi_{\sigma}) d\mathbf{r}, \quad (27)$$

where $\varepsilon_{X,\sigma}^{\text{LSDA}}$ is the LSDA exchange-energy density,

$$\chi_{\sigma} = \frac{|\nabla \rho_{\sigma}|}{\rho_{\sigma}^{4/3}} \quad (28)$$

is the reduced density gradient, and $F(\chi_{\sigma})$ is the enhancement factor. This factor serves to increase the contribution to the exchange energy, beyond that seen with the LSDA, for the large gradient regions that occur in finite molecular systems. The behavior of various GGAs (and their ensuing hybrids) for dispersion-bound systems can be directly linked to differences in the large-gradient limits of their enhancement factors.^{87–95}

Figure 7a shows the exchange enhancement factors of the popular BLYP^{83,120} and PBE⁸⁵ functionals, along with the B86b exchange functional.⁸¹ The optimal behavior of the enhancement factor for accurate treatment of nonbonded repulsion is to have a large-gradient limit that diverges as $\chi_{\sigma}^{2/5}$, which is obeyed by the PW86⁸² and B86b⁸¹ GGAs. The combination of B86b exchange with the PBE correlation functional⁸⁵ (B86bPBE) is our group's GGA of choice,⁹⁵ although the PBE exchange-correlation functional is vastly more popular. BLYP^{83,120} gives a large-gradient limit that diverges too quickly, while the PBE⁸⁵ enhancement factor approaches a constant, as they were each designed to obey different constraints. While some researchers prefer “dispersionless” exchange functionals^{95,236} that provide an accurate description of nonbonded repulsion, another strategy in development of DFAs is to attempt to capture “intermediate-range” dispersion through the exchange functional.^{237–239} This is based on the principle that local and semi-local exchange functionals already mimic nondynamical (or static) correlation and is prevalent in the development of meta-GGAs, such as the Minnesota functionals and SCAN.

To illustrate the connection between enhancement factor and treatment of nonbonded repulsion, Figure 7b shows computed potential energy surfaces for the dispersion-bound methane dimer. In the absence of a dispersion correction, BLYP gives a PES that is far too repulsive compared to HF theory, while PBE gives a PES that is too attractive. Thus, the shifts in the PES, relative to the HF reference curve, follow the same ordering as the large-gradient limits of the enhancement factors.

Given the above, it is clear that, in cases where the description of nonbonded repulsion affects the thermochemistry, mixing in some fraction of exact exchange can reduce errors seen with common GGAs, even without significant SIE. As an example, we consider the “DARC” benchmark of 10 Diels–Alder reaction energies from the GMTKN data set.¹⁰⁹ In these reactions, there is a loss of π -conjugation in going from the reactants to the products, so delocalization error is expected to play some role.²⁴⁰ However, treatment of nonbonded repulsion is much more important for these addition reactions.²⁴⁰ This can be clearly seen by contrasting the BLYP and PBE results in Table 3. If SIE were the dominant error, then we would expect to see similar performance for both functionals, as for the H_2^+ and He_2^+ PES in Figure 1.

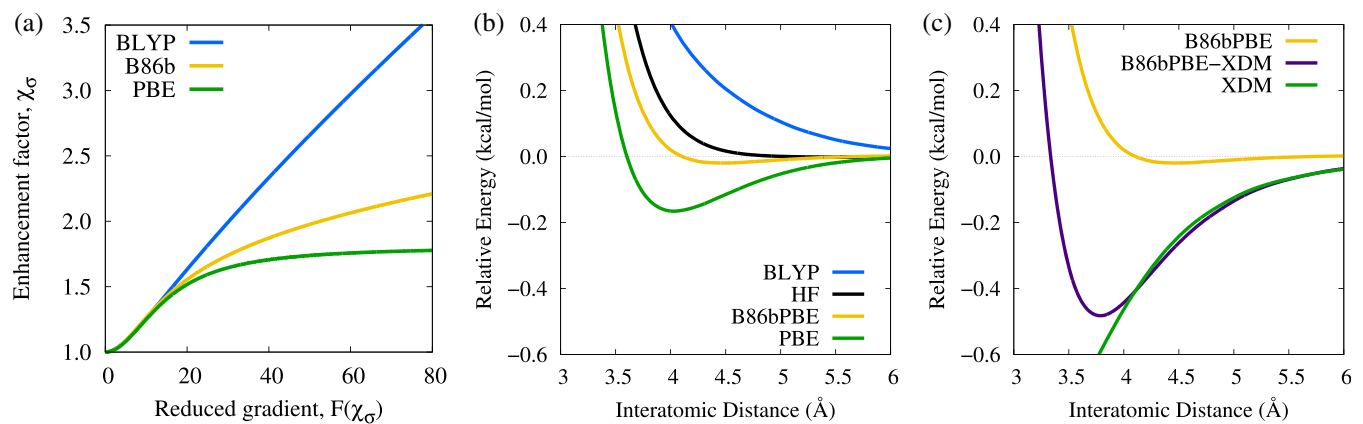


FIGURE 7 Behavior of the GGA enhancement factor for selected functionals (a). Also shown are potential energy curve for the methane dimer (b) with selected methods computed using FHIaims¹⁷⁴ with tight settings for the DFT calculations and Gaussian¹³⁷ with the aug-cc-pVTZ basis set for HF.¹³⁷ Panel (c) illustrates the effect of the XDM dispersion correction; for comparison, the reference CCSD(T) binding energy of the methane dimer is 0.53 kcal/mol.²³⁵

TABLE 3 Mean absolute errors (in kcal/mol) for several literature benchmarks obtained using selected functionals with and without a dispersion correction. Mean errors are given in parentheses, with negative values indicating overbinding. All calculations were performed using the aug-cc-pVTZ basis set (except for the XB benchmark, which used aug-cc-pVQZ) with Gaussian 16¹³⁷ (psi4¹³⁸ for the SCAN calculations).

Functional	Dispersion	DARC ¹⁰⁹	S66 ^{241,242}	HB ²⁴³	XB ^{59,219}
BLYP	None	23.1	(23.1)	4.07	(4.07)
	D3(BJ)	13.7	(13.7)	0.23	(−0.09)
B3LYP	None	15.3	(15.3)	3.16	(3.16)
	D3(BJ)	7.5	(7.5)	0.34	(−0.33)
PBE	None	6.8	(6.6)	2.08	(2.08)
	D3(BJ)	3.2	(2.0)	0.32	(−0.27)
SCAN	None	2.4	(0.1)	0.76	(0.52)
	D3(BJ)	1.9	(−1.2)	0.45	(−0.43)
PBE0	None	3.0	(0.2)	1.98	(1.97)
	D3(BJ)	4.0	(−4.0)	0.33	(−0.31)
LC- ω PBE	None	6.2	(−6.2)	2.42	(2.42)
	D3(BJ)	10.8	(−10.8)	0.26	(−0.10)

However, while both GGAs systematically under-bind the addition products, the errors in Table 3 are three to four times larger for BLYP than for PBE due to overestimation of non-bonded repulsion by BLYP. Based only on the improvement from BLYP to B3LYP, one might conjecture that SIE is the dominant source of error for these reactions, but this is not reflected in the good performance of dispersion-corrected PBE and SCAN. Finally, the large error seen with LC- ω PBE for the addition reactions is most likely due to poor transferability of the range-separation parameter between the small-molecule reactants and the much larger products. As highlighted previously, tuning of an optimal range-separation parameter is dependent on system size.^{172,196,198}

4.2 | Dispersion corrections and performance for intermolecular benchmarks

Almost all DFAs (including the LSDA, GGAs, meta-GGAs, global and range-separated hybrids) include only local or semi-local ingredients to model electron correlation and, hence, do not include the requisite physics to model London dispersion.⁹⁵ While some DFAs mimic dispersion-like binding at short intermolecular distances, this is a spurious

attraction arising from the exchange functional rather than a physically meaningful representation of dispersion, and the correct $-C_6/R^6$ asymptotic behavior is lacking. Thus, most DFAs should be paired with a dispersion correction. Dispersion can be effectively modeled by an additive post-SCF correction to the DFT energy, as is done for the Grimme,^{218,244} Tkatchenko–Scheffler,²⁴⁵ many-body,^{246,247} or our own exchange-hole dipole moment (XDM),^{248–251} dispersion corrections. Alternatively, explicitly nonlocal DFA models of dispersion can be used, as in the vdW-DF2^{252,253} and rVV10²⁵⁴ functionals. The importance of a dispersion correction is emphasized in Figure 7c for the methane dimer and by the MAEs in Table 3 for the S66 set^{241,242} of van der Waals (vdW) complexes. We selected D3(BJ) for all examples in Tables 1–3 since it is the most popular option with users of molecular DFT.

In all cases, the dispersion correction adds necessary physics missing from the underlying DFA and should not be viewed as optional. However, there have been reports of dispersion corrections worsening performance for certain benchmarks,^{219,229} so dispersion is unfortunately not always included in production DFA calculations on intermolecular complexes or on large molecular systems, where it can significantly impact the chemistry. The reason for the apparent contradiction of dispersion corrections worsening results is due to the interplay between dispersion with both the exchange enhancement factor and delocalization error. The differing behavior of base DFAs for nonbonded repulsion explains why additive dispersion corrections should be parameterized individually for use with a given functional to benefit from error cancellation.¹⁰⁹

Dispersion is an attractive interaction and will always stabilize vdW dimers, supermolecular complexes, and molecular crystals, to list only a few examples. However, if these systems are already overstabilized because of delocalization error or an exchange functional that already mimics intermediate-range dispersion-like binding, then adding a dispersion correction will increase the extent of the error. Examples are shown in Table 3 for the Water20 hydrogen-bonding benchmark²⁴³ (HB) and Bauza's halogen-bonding benchmark^{59,219} (XB).

The Water20 results can be explained by the exchange enhancement factor. BLYP and B3LYP are overly repulsive, so adding dispersion decreases their MAEs; this actually changes the sign of the overall error and leads to overbinding due to delocalization error since GGAs are known to excessively polarize co-operative hydrogen-bonding networks.^{94,95,163,217,255} On the other hand, PBE and SCAN are already overly attractive without dispersion. For both these functionals, and for PBE0, which coincidentally gives quite good performance for H-bonds in the absence of dispersion, adding a dispersion correction increases the MAEs. Finally, LC- ω PBE provides a reasonable description of nonbonded repulsion and minimal delocalization error, so adding dispersion once again improves the results, providing the lowest MAE.

In Section 3.3, we saw that there is significant density-driven delocalization error for the halogen-bonding benchmark, where GGAs predict excessive charge transfer. Thus, delocalization error leads to overbinding of the halogen-bonded complexes with PBE, SCAN, and PBE0, so adding a dispersion correction once again increases the error. As LC- ω PBE has minimal delocalization error, adding dispersion improves performance. Dispersion also slightly improves performance for BLYP and B3LYP, as the errors in these functionals for non-bonded repulsion partially offset the delocalization error.

In summary, when selecting a DFA, it is important to choose based on inclusion of appropriate physics and the interested reader is directed to our perspective on requirements for an accurate dispersion-corrected DFA.⁹⁵ Care must be taken not to simply choose a DFA based on good performance for one or two literature benchmarks when this may be entirely due to fortuitous error cancellation.

5 | OUTLOOK: METHOD CHOICES AND ONGOING DFA DEVELOPMENT

Now that we have reviewed the origins of delocalization error, its decomposition into energy-driven and density-driven contributions, and its interplay with dispersion corrections, what strategies should be taken to reduce it in production calculations? The most straightforward method to reduce delocalization error is use of hybrid or range-separated hybrid functionals. The improvement in properties going from GGAs to conventional hybrids with 20–25% exact exchange, to hybrids with near 50% exact exchange, is the typical indicator of systems with significant SIE. The drawback here is that one must recognize when delocalization error is important in a system and choose a hybrid functional accordingly. As stated previously, a dispersion correction should be paired with all such DFAs to model important, otherwise missing, physics.

Beyond global hybrids, range-separated hybrids with full long-range exact exchange provided the first functionals that can be free of N -electron SIE and these are the most accurate DFAs in common use today.^{109,113} The limitation of

range-separated functionals is that the optimal range separation is highly system dependent,^{172,184,196–198} so a single parameterization cannot be used across main-group and transition-metal chemistry, or for a mix of large and small molecules, with the expectation of full transferability. Additionally, any amount of long-range exact exchange in global or range-separated hybrids is not recommended for bulk metals or small-gap semi-conductors.

Even more accurate than range-separated hybrids for finite molecules are double hybrids,^{256–262} which include correlation-energy terms based on MP2 theory. The use of nonlocal MP2 correlation is conducive to higher exact-exchange mixing fractions and, hence, almost entirely eliminates delocalization error. However, due to the inclusion of MP2 correlation, the energy depends on the unoccupied (virtual) KS orbitals and, consequently, double hybrids are not true density functionals. By a strict definition, a DFA energy should depend on properties of the electron density and occupied orbitals only.⁷³ Inclusion of the MP2 correlation term leads to two unfavorable consequences. The first is that it degrades the scaling with system size, inhibiting application of double hybrids to very large systems. The second is that double hybrids can perform poorly in cases where MP2 has well-known failures, including susceptibility to spin contamination²³⁰ (albeit to a much lesser extent than MP2 itself for organic radicals²⁶³) and divergence of the energy for small HOMO-LUMO gaps, as occur for highly stretched bonds.^{264,265} Similarly to global or range-separated hybrids, double hybrids are not recommended for bulk solids and, due to the zero band gap, will diverge for metals. The solid-state analogue of double-hybrid functionals is the random-phase approximation (RPA). RPA-based methods^{266–271} have also shown great promise at reducing delocalization error but, again, their high computational cost makes them less practical for large systems or crystals with large unit cells.

For very large systems, or for solid-state calculations using plane-wave basis sets, even hybrid calculations can be prohibitively expensive, so methods to reduce delocalization error while maintaining GGA cost are needed. These include Fermi–Löwdin-orbital SIC^{139,153,156–158} and LOSC,^{200–202} as discussed in Sections 2.3 and 2.4, respectively. Another possibility is “rung 3.5” functionals,^{272–275} so named because they are intermediate between meta-GGAs and hybrids in terms of accuracy. These functionals quantify delocalization by projecting the density matrix formed from the KS orbitals on a set Gaussian-type orbital of atomic size. This projection is done for every reference point on the integration grid and incorporated into the exchange-correlation energy expression, serving as a correction for fractional charges.

Some alternative low-cost strategies are targeted to more niche applications than to computations across the full breadth of chemistry. One approach targeting transition metals is the addition of a Hubbard U term^{276–283} to the exchange-correlation energy that serves to shift the orbital energies of the d or f electrons, preventing hybridization. While GGA + U methods are capable of high accuracy for metal-containing systems, this approach is not transferable to other manifestations of delocalization error. Another approach is the use of optimized effective potential methods, such as TB-mBJ,^{284,285} where one models the exchange-correlation potential rather than the exchange-correlation energy. Such methods can significantly improve predictions of the band gap.^{286–291} However, as they only provide single-particle (orbital) energies, and not a well-defined total energy expression, they are not applicable to thermochemistry.

The final class of functionals we will discuss is those that depend on the exact exchange-energy density (ϵ_X^{HF}).^{4,14,15,178,292–296} These include local hybrid functionals,^{179,297–303} in which the exact-exchange mixing is position dependent:

$$E_X^{\text{LH}} = \int a_X(\mathbf{r}) \epsilon_X^{\text{HF}} d\mathbf{r} + \int [1 - a_X(\mathbf{r})] \epsilon_X^{\text{DFA}} d\mathbf{r}, \quad (29)$$

where the mixing, $a_X(\mathbf{r})$, can be a functional of the density and its derivatives. Alternatively, Becke^{4,14,178} has developed real-space density-functional models of electron correlation that, unlike semi-local DFA correlation functionals, are designed to pair with full exact exchange. Here, the energy is a sum of the HF exchange and the real-space correlation energy, where the latter involves a sum over dynamical,³⁰⁴ non-dynamical,^{4,178} and perhaps strong,¹⁴ correlation-energy terms. The correlation energies themselves are complicated functionals of the density, its derivatives, and the exact exchange-energy density. While this class of functionals is perhaps the most promising avenue for consistent elimination of delocalization error,^{32,305,306} their form has typically made self-consistent implementation impractical, which has all but prohibited their use in production calculations.

The first functional employing the exact exchange-energy density to have a practical and open-source self-consistent implementation is DeepMind 2021 (DM21), which is a local, range-separated hybrid functional developed by Kirkpatrick et al.³⁰⁷ By training a deep neural network on small main-group molecules (containing elements from

H-Kr), in addition to fractional-charge and fractional-spin constraints for H-Ar atoms, this functional attempts to correct delocalization and multireference errors for a variety of chemical systems. The input features to the neural network include the spin-indexed density ρ , $|\nabla\rho|$, the kinetic energy density τ , and the range-separated exact exchange energy densities $\varepsilon_X^{\text{HF}}$, and $\varepsilon_X^{\omega\text{HF}}$. As one would expect, DM21 outperforms existing global hybrids in challenging systems due to its dynamic mixing of exact exchange.³⁰⁸ While this functional has shown exceptional performance for a number of molecular benchmarks,^{109,307–310} it has not been trained for transition-metal chemistry, extended systems, liquids, or solids.³¹¹

All of the areas discussed here are highly fruitful ground for ongoing functional development and the above is by no means a comprehensive list of DFA-based approaches to reduce delocalization error. However, despite decades of research effort, a DFA that is free of delocalization error, has consistently high accuracy, and is generally applicable to molecular and solid-state chemistry is still tantalizingly out of reach. In our opinion, resolving delocalization error remains the greatest outstanding challenge in DFT today.

AUTHOR CONTRIBUTIONS

Kyle R. Bryenton: Data curation (equal); visualization (equal); writing – review and editing (equal). **Adebayo A. Adeleke:** Data curation (equal); visualization (equal); writing – review and editing (equal). **Stephen G. Dale:** Data curation (equal); visualization (equal); writing – review and editing (equal). **Erin R. Johnson:** Conceptualization (lead); data curation (equal); visualization (equal); writing – original draft (lead); writing – review and editing (equal).

ACKNOWLEDGMENTS

This research was funded by the Natural Sciences and Engineering Research Council of Canada (NSERC). The authors are grateful to ACENET and Compute Canada for computational resources. We also thank the Killam Trust and the Walter C. Sumner Foundation for fellowships to Kyle R. Bryenton. Stephen G. Dale would like to acknowledge the support of the Australian Government through the Australian Research Council (project number DP200100033).

CONFLICT OF INTEREST

The authors have declared no conflicts of interest for this article.

DATA AVAILABILITY STATEMENT

Data available on request from the authors.

ORCID

Kyle R. Bryenton  <https://orcid.org/0000-0001-5716-5314>

Adebayo A. Adeleke  <https://orcid.org/0000-0002-9057-431X>

Stephen G. Dale  <https://orcid.org/0000-0002-6867-711X>

Erin R. Johnson  <https://orcid.org/0000-0002-5651-468X>

RELATED WIREs ARTICLES

[Long-range correction for density functional theory](#)

[On the top rung of Jacob's ladder of density functional theory: Toward resolving the dilemma of SIE and NCE](#)

[Density functional theory with London dispersion corrections](#)

REFERENCES

1. Kohn W, Sham LJ. Self-consistent equations including exchange and correlation effects. *Phys Rev A*. 1965;140:1133–8.
2. van Noorden R, Maher B, Nuzzo R. The top 100 papers. *Nature*. 2014;514:550–3.
3. Ziegler T, Rauk A, Baerends EJ. Calculation of multiplet energies by the Hartree-Fock-Slater method. *Theor Chim Acta*. 1977;43: 261–71.
4. Becke AD. A real-space model of nondynamical correlation. *J Chem Phys*. 2003;119:2972–7.
5. Cohen AJ, Mori-Sánchez P, Yang W. Fractional spins and static correlation error in density functional theory. *J Chem Phys*. 2008;129: 121104.
6. Cohen AJ, Mori-Sánchez P, Yang W. Challenges for density functional theory. *Chem Rev*. 2011;112:289–320.
7. Ess DH, Johnson ER, Hu X, Yang W. Singlet-triplet energy gaps for diradicals from fractional-spin density-functional theory. *J Phys Chem A*. 2011;115:76–83.
8. Hollett JW, Gill PMW. The two faces of static correlation. *J Chem Phys*. 2011;134:114111.

9. Fogueri UR, Kozuch S, Karton A, Martin JML. A simple DFT-based diagnostic for nondynamical correlation. *Theor Chem Acc.* 2013; 132:1291.
10. Grimme S, Waletzke M. A combination of Kohn-Sham density functional theory and multi-reference configuration interaction methods. *J Chem Phys.* 1999;111:5645–55.
11. Gräfenstein J, Cremer D. Can density functional theory describe multi-reference systems? Investigation of carbenes and organic biradicals. *Phys Chem Chem Phys.* 2000;2:2091–103.
12. Slipchenko LV, Krylov AI. Singlet-triplet gaps in diradicals by the spin-flip approach: a benchmark study. *J Chem Phys.* 2002;117: 4694–708.
13. Peng D, Hu X, Devarajan D, Ess DH, Johnson ER, Yang W. Variational fractional-spin density-functional theory for Diradicals. *J Chem Phys.* 2012;137:114112.
14. Becke AD. Density functionals for static, dynamical, and strong correlation. *J Chem Phys.* 2013;138:074109.
15. Kong J, Proynov E. Density functional model for nondynamic and strong correlation. *J Chem Theory Comput.* 2016;12:133–43.
16. Laqua H, Kussmann J, Ochsenfeld C. Density functional theory model for multi-reference systems based on the exact-exchange hole normalization. *J Chem Phys.* 2018;148:121101.
17. Wodyński A, Arbuznikov AV, Kaupp M. Local hybrid functionals augmented by a strong-correlation model. *J Chem Phys.* 2021;155: 144101.
18. Filatov M, Shaik S. A spin-restricted ensemble-referenced Kohn-Sham method and its application to diradicaloid situations. *Chem Phys Lett.* 1999;304:429–37.
19. Filatov M, Huix-Rotllant M, Burghardt I. Ensemble density functional theory method correctly describes bond dissociation, excited state electron transfer, and double excitations. *J Chem Phys.* 2015;142:184104.
20. Filatov M. Spin-restricted ensemble-referenced Kohn-Sham method: basic principles and application to strongly correlated ground and excited states of molecules. *WIREs Comput Mol Sci.* 2015;5:146–67.
21. Filatov M. In: Ferré N, Filatov M, Huix-Rotllant M, editors. *Ensemble DFT approach to excited states of strongly correlated molecular systems.* Cham: Springer International Publishing; 2016. p. 97–124.
22. Gould T, Pittalis S. Hartree and exchange in ensemble density functional theory: avoiding the nonuniqueness disaster. *Phys Rev Lett.* 2017;119:243001.
23. Gould T, Stefanucci G, Pittalis S. Ensemble density functional theory: insight from the fluctuation-dissipation theorem. *Phys Rev Lett.* 2020;125:233001.
24. Gould T, Kronik L, Pittalis S. Double excitations in molecules from ensemble density functionals: theory and approximations. *Phys Rev A.* 2021;104:022803.
25. Chermette H, Ciofini I, Mariotti F, Daul C. Correct dissociation behavior of radical ions such as H_2^+ in density functional calculations. *J Chem Phys.* 2001;114:1447–53.
26. Grafenstein J, Kraka E, Cremer D. The impact of the self-interaction error on the density functional theory description of dissociating radical cations: ionic and covalent dissociation limits. *J Chem Phys.* 2004;120:524–39.
27. Ruzsinszky A, Perdew JP, Csonka GI. Binding energy curves from nonempirical density functionals. I. Covalent bonds in closed-shell and radical molecules. *J Phys Chem A.* 2005;109:11006–14.
28. Janesko BG, Proynov E, Kong J, Scalmani G, Frisch MJ. Practical density functionals beyond the overdelocalization-underbinding zero-sum game. *J Phys Chem Lett.* 2017;8:4314–8.
29. Ruiz E, Salahub DR, Vela A. Charge-transfer complexes: stringent tests for widely used density functionals. *J Chem Phys.* 1996;100: 12265–76.
30. Sini G, Sears JS, Bredas JL. Evaluating the performance of DFT functionals in assessing the interaction energy and ground-state charge transfer of donor/acceptor complexes: tetrathiafulvalene-tetracyanoquinodimethane (TTF-TCNQ) as a model case. *J Chem Theory Comput.* 2011;7:602–9.
31. Steinmann SN, Piemontesi C, Delacht A, Corminboeuf C. Why are the interaction energies of charge-transfer complexes challenging for DFT? *J Chem Theory Comput.* 2012;8:1629–40.
32. Becke AD, Dale SG, Johnson ER. Correct charge transfer in CT complexes from the Becke'05 density functional. *J Chem Phys.* 2018; 148:211101.
33. Lynch BJ, Truhlar DG. How well can hybrid density functional methods predict transition state geometries and barrier heights? *J Phys Chem A.* 2001;105:2936–41.
34. Csonka GI, Johnson BG. Inclusion of exact exchange for self-interaction corrected H3 density functional potential energy surface. *Theor Chem Acc.* 1998;99:158–65.
35. Patchkovskii S, Ziegler T. Improving “difficult” reaction barriers with self-interaction corrected density functional theory. *J Chem Phys.* 2002;116:7806–13.
36. Dickson RM, Becke AD. Reaction barrier heights from an exact-exchange-based density-functional correlation model. *J Chem Phys.* 2005;123:111101.
37. Lingwood M, Hammond JR, Hrovat DA, Mayer JM, Borden WT. MPW1K performs much better than B3LYP in DFT calculations on reactions that proceed by proton-coupled electron transfer (PCET). *J Chem Theory Comput.* 2006;2:740–5.
38. Janesko BG, Scuseria GE. Hartree-Fock orbitals significantly improve the reaction barrier heights predicted by semilocal density functionals. *J Chem Phys.* 2008;128:244112.

39. Sham LJ, Schlüter M. Density-functional theory of the band gap. *Phys Rev B*. 1985;32:3883–9.
40. Perdew JP. Density functional theory and the band gap problem. *Int J Quantum Chem*. 1985;28:497–523.
41. Cohen AJ, Mori-Sánchez P, Yang W. Fractional charge perspective on the band gap in density-functional theory. *Phys Rev B*. 2008;77:115123.
42. Mori-Sánchez P, Cohen AJ, Yang W. Localization and delocalization errors in density functional theory and implications for band-gap prediction. *Phys Rev Lett*. 2008;100:146401.
43. Crowley JM, Tahir-Kheli J III, WAG. Resolution of the band gap prediction problem for materials design. *J Phys Chem Lett*. 2016;7:1198–203.
44. Perdew JP, Yang W, Burke K, Yang Z, Gross EKU, Scheffler M, et al. Understanding band gaps of solids in generalized Kohn-Sham theory. *Proc Nat Acad Sci*. 2017;114:2801–6.
45. McDowell SAC, Amos RD, Handy NC. Molecular polarisabilities - a comparison of density functional theory with standard ab initio methods. *Chem Phys Lett*. 1995;235:1–4.
46. Champagne B, Perpète EA. Assessment of conventional density functional schemes for computing the polarizabilities and hyperpolarizabilities of conjugated oligomers: an ab initio investigation of polyacetylene chains. *J Chem Phys*. 1998;109:10489–98.
47. Mori-Sánchez P, Wu Q, Yang W. Accurate polymer polarizabilities with exact exchange density-functional theory. *J Chem Phys*. 2003;119:11001–4.
48. Jacquemin D, Perpète EA, Scalmani G, Frisch MJ, Kobayashi R, Co A. Assessment of the efficiency of long-range corrected functionals for some properties of large compounds. *J Chem Phys*. 2007;126:144105.
49. Sancho-García JC, Pérez-Jiménez AJ, Moscardo F. Description of C(sp²)-C(sp²) rotation in butadiene by density functionals. *J Phys Chem A*. 2001;105:11541–8.
50. Woodcock HL, Schaefer HF, Schreiner PR. Problematic energy differences between cumulenes and poly-ynes: does this point to a systematic improvement of density functional theory? *J Phys Chem A*. 2002;106:11923–31.
51. Cai ZL, Sendt K, Reimers JR. Failure of density-functional theory and time-dependent density-functional theory for large extended π systems. *J Chem Phys*. 2002;117:5543–9.
52. Johnson ER, Clarkin OJ, DiLabio GA. Density functional theory based model calculations for accurate bond dissociation enthalpies. 3. A single approach for XH, XX, and XY (X, Y= C, N, O, S, halogen) bonds. *J Phys Chem A*. 2003;107:9953–63.
53. Jacquemin D, Femenias A, Chermette H, Ciofini I, Adamo C, André JM, et al. Assessment of several hybrid DFT functionals for the evaluation of bond length alternation of increasingly long oligomers. *J Phys Chem A*. 2006;110:5952–9.
54. Heaton-Burgess T, Yang W. Structural manifestation of the delocalization error of density functional approximations: C_{4N+2} rings and C₂₀ bowl, cage, and ring isomers. *J Chem Phys*. 2010;132:234113.
55. White MA, Kahwaji S, Freitas VLS, Siewert R, Weatherby JA, Ribeiro da Silva MDMC, et al. Relative thermodynamic stability of diamond and graphite. *Angew Chem Int Ed*. 2021;60:1546–9.
56. Nam S, Cho E, Sim E, Burke K. Explaining and fixing DFT failures for torsional barriers. *J Phys Chem Lett*. 2021;12:2796–804.
57. Greenwell C, Beran GJO. Inaccurate conformational energies still hinder crystal structure prediction in flexible organic molecules. *Cryst Growth Des*. 2020;20:4875–2881.
58. Beran GJ, Sugden IJ, Greenwell C, Bowskill D, Pantelides CC, A djiman C. How many more polymorphs of ROY remain undiscovered? *Chem Sci*. 2022;13:1288–97.
59. Otero-de-la-Roza A, Johnson ER, DiLabio GA. Halogen bonding from dispersion-corrected density-functional theory: the role of delocalization error. *J Chem Theory Comput*. 2014;10:5436–47.
60. Kim Y, Song S, Sim E, Burke K. Halogen and chalcogen binding dominated by density-driven errors. *J Phys Chem Lett*. 2019;10:295–301.
61. Mehta N, Fellowes T, White JM, Goerigk L. CHAL336 benchmark set: how well do quantum-chemical methods describe Chalcogen-bonding interactions? *J Chem Theory Comput*. 2021;17:2783–806.
62. LeBlanc LM, Dale SG, Taylor CR, Becke AD, Day GM, Johnson ER. Pervasive delocalisation error causes spurious proton transfer in organic acid-base co-crystals. *Angew Chem Int Ed*. 2018;57:14906–10.
63. Perdew JP, Zunger A. Self-interaction correction to density-functional approximations for many-electron systems. *Phys Rev B*. 1981;23:5048–79.
64. Perdew JP, Parr RG, Levy M, Balduz JL. Density-functional theory for fractional particle number - derivative discontinuities of the energy. *Phys Rev Lett*. 1982;49:1691–4.
65. Mori-Sánchez P, Cohen AJ, Yang W. Many-electron self-interaction error in approximate density functionals. *J Chem Phys*. 2006;125:201102.
66. Ruzsinszky A, Perdew JP, Csonka GI, Vydrov OA, Scuseria GE. Spurious fractional charge on dissociated atoms: pervasive and resilient self-interaction error of common density functionals. *J Chem Phys*. 2006;125:194112.
67. Cohen AJ, Mori-Sánchez P, Yang W. Insights into current limitations of density functional theory. *Science*. 2008;321:792–4.
68. Zhang Y, Yang W. Perspective on “Density-functional theory for fractional particle number: derivative discontinuities of the energy”. *Theoretical chemistry accounts*. Berlin: Springer; 2000. p. 346–8.
69. Henderson TM, Janesko BG, Scuseria GE. Range separation and local hybridization in density functional theory. *J Phys Chem A*. 2008;112:12530–42.
70. Perdew JP, Ruzsinszky A, Constantin LA, Sun J, Csonka GI. Some fundamental issues in ground-state density functional theory: a guide for the perplexed. *J Chem Theory Comput*. 2009;5:902–8.

71. Ruzsinszky A, Perdew JP. Twelve outstanding problems in ground-state density functional theory: a bouquet of puzzles. *Comput Theor Chem.* 2011;963:2–6.
72. Burke K. Perspective on density functional theory. *J Chem Phys.* 2012;136:150901.
73. Becke AD. Fifty years of density-functional theory in chemical physics. *J Chem Phys.* 2014;140:18A301.
74. Janesko BG. Replacing hybrid density functional theory: motivation and recent advances. *Chem Soc Rev.* 2021;50:8470–95.
75. Hohenberg P, Kohn W. Inhomogeneous electron gas. *Phys Rev.* 1964;136:B864–71.
76. Slater JC. The self-consistent field for molecular and solids, quantum theory of molecular and solids. Vol 4. New York: McGraw-Hill; 1974.
77. Becke AD. Completely numerical calculations on diatomic molecules in the local-density approximation. *Phys Rev A.* 1986;33: 2786–8.
78. Vosko SH, Wilk L, Nusair M. Accurate spin-dependent electron liquid correlation energies for local spin density calculations: a critical analysis. *Can J Phys.* 1980;58:1200–11.
79. Becke AD. A multicenter numerical integration scheme for polyatomic molecules. *J Chem Phys.* 1988;88:2547–53.
80. Becke AD. Density functional calculations of molecular bond energies. *J Chem Phys.* 1986;85:4524–9.
81. Becke AD. On the large-gradient behavior of the density functional exchange energy. *J Chem Phys.* 1986;85:7184–7.
82. Perdew JP, Yue W. Accurate and simple density functional for the electronic exchange energy: generalized gradient approximation. *Phys Rev B.* 1986;33:8800–2.
83. Becke AD. Density-functional exchange-energy approximation with correct asymptotic behavior. *Phys Rev A.* 1988;38:3098–100.
84. Perdew JP, Chevary JA, Vosko SH, Jackson KA, Pederson MR, Singh DJ, et al. Atoms, molecules, solids, and surfaces: applications of the generalized gradient approximation for exchange and correlation. *Phys Rev B.* 1992;46:6671–87.
85. Perdew JP, Burke K, Ernzerhof M. Generalized gradient approximation made simple. *Phys Rev Lett.* 1996;77:3865–8.
86. Perdew JP, Ruzsinszky A, Csonka GI, Vydrov OA, Scuseria GE, Constantin LA, et al. Restoring the density-gradient expansion for exchange in solids and surfaces. *Phys Rev Lett.* 2008;100:136406.
87. Lacks DJ, Gordon RG. Pair interactions of rare-gas atoms as a test of exchange-energy-density functionals in regions of large density gradients. *Phys Rev A.* 1993;47:4681–90.
88. Perez-Jorda JM, Becke AD. A density-functional study of van-der-Waals forces – rare-gas diatomics. *Chem Phys Lett.* 1995;233:134–7.
89. Zhang Y, Pan W, Yang W. Describing van der Waals interaction in diatomic molecules with generalized gradient approximations: the role of the exchange functional. *J Chem Phys.* 1997;107:7921–5.
90. Kannemann FO, Becke AD. Van der Waals interactions in density-functional theory: rare-gas diatomics. *J Chem Theory Comput.* 2009;5:719–27.
91. Johnson ER, Wolkow RA, DiLabio GA. Application of 25 density functionals to dispersion-bound homomolecular dimers. *Chem Phys Lett.* 2004;394:334–8.
92. Murray ÉD, Lee K, Langreth DC. Investigation of exchange energy density functional accuracy for interacting molecules. *J Chem Theory Comput.* 2009;5:2754–62.
93. Gillan MJ. Many-body exchange-overlap interactions in rare gases and water. *J Chem Phys.* 2014;141:224106.
94. Otero-de-la-Roza A, DiLabio GA, Johnson ER. Exchange-correlation effects for noncovalent interactions in density functional theory. *J Chem Theory Comput.* 2016;12:3160–75.
95. Price AJA, Bryenton KR, Johnson ER. Requirements for an accurate dispersion-corrected density functional. *J Chem Phys.* 2021;154: 230902.
96. Becke AD, Roussel MR. Exchange holes in inhomogeneous systems – a coordinate-space model. *Phys Rev A.* 1989;39:3761–7.
97. Becke AD. Density-functional thermochemistry. 4. A new dynamical correlation functional and implications for exact-exchange mixing. *J Chem Phys.* 1996;104:1040–6.
98. Becke AD. A new inhomogeneity parameter in density-functional theory. *J Chem Phys.* 1998;109:2092–8.
99. Perdew JP, Kurth S, Zupan A, Blaha P. Accurate density functional with correct formal properties: a step beyond the generalized gradient approximation. *Phys Rev Lett.* 1999;82:2544–7.
100. Adamo C. The meta-GGA functional: thermochemistry with a kinetic energy density dependent exchange-correlation functional. *J Chem Phys.* 2000;112:2643–9.
101. Tao J, Perdew JP, Staroverov VN, Scuseria GE. Climbing the density functional ladder: nonempirical meta-generalized gradient approximation designed for molecules and solids. *Phys Rev Lett.* 2003;91:146401.
102. Zhao Y, Truhlar DG. A new local density functional for main-group thermochemistry, transition metal bonding, thermochemical kinetics, and noncovalent interactions. *J Chem Phys.* 2006;125:194101.
103. Peverati R, Truhlar DG. M11-L: a local density functional that provides improved accuracy for electronic structure calculations in chemistry and physics. *J Phys Chem Lett.* 2012;3:117–24.
104. Yu HS, He X, Truhlar DG. MN15-L: a new local exchange-correlation functional for Kohn-Sham density functional theory with broad accuracy for atoms, molecules, and solids. *J Chem Theory Comput.* 2016;12:1280–93.
105. Sun J, Ruzsinszky A, Perdew JP. Strongly constrained and appropriately normed Semilocal Density functional. *Phys Rev Lett.* 2015; 115:036402.
106. Furness JW, Kaplan AD, Ning J, Perdew JP, Sun J. Accurate and numerically efficient r^2 SCAN meta-generalized gradient approximation. *J Phys Chem Lett.* 2020;11:8208–15.

107. Becke AD, Edgecombe KE. A simple measure of electron localization in atomic and molecular-systems. *J Chem Phys.* 1990;92:5397–403. <https://doi.org/10.1063/1.458517>
108. Schmider HL, Becke AD. Chemical content of the kinetic energy density. *J Mol Struct Theochem.* 2000;527:51–61. [https://doi.org/10.1016/S0166-1280\(00\)00477-2](https://doi.org/10.1016/S0166-1280(00)00477-2)
109. Goerigk L, Hansen A, Bauer C, Ehrlich S, Najibi A, Grimme S. A look at the density functional theory zoo with the advanced GMTKN55 database for general main group thermochemistry, kinetics and noncovalent interactions. *Phys Chem Chem Phys.* 2017;19: 32184–215.
110. Ehlert S, Huniar U, Ning J, Furness JW, Sun J, Kaplan AD, et al. r^2 SCAN-D4: dispersion corrected meta-generalized gradient approximation for general chemical applications. *J Chem Phys.* 2021;154:061101.
111. Goerigk L, Grimme S. A thorough benchmark of density functional methods for general main group thermochemistry, kinetics, and noncovalent interactions. *Phys Chem Chem Phys.* 2011;13:6670–88.
112. Medvedev MG, Bushmarinov IS, Sun J, Perdew JP, Lyssenko KA. Density functional theory is straying from the path toward the exact functional. *Science.* 2017;355:49–52.
113. Mardirossian N, Head-Gordon M. Thirty years of density functional theory in computational chemistry: an overview and extensive assessment of 200 density functionals. *Mol Phys.* 2017;115:2315–72.
114. Hait D, Head-Gordon M. Delocalization errors in density functional theory are essentially quadratic in fractional occupation number. *J Phys Chem Lett.* 2018;9:6280–8.
115. Modrzejewski M, Chalasinski G, Szczesniak MM. Assessment of newest meta-gga hybrids for late transition metal reactivity: fractional charge and fractional spin perspective. *J Phys Chem C.* 2018;123:8047–56.
116. Sai Gautam G, Carter EA. Evaluating transition metal oxides within DFT-SCAN and SCAN+U frameworks for solar thermochemical applications. *Phys Rev Mater.* 2018;2:095401.
117. Long OY, Gautam GS, Carter EA. Evaluating optimal U for 3 d transition-metal oxides within the SCAN+ U framework. *Phys Rev Mater.* 2020;4:045401.
118. Becke AD. A new mixing of Hartree–Fock and local density-functional theories. *J Chem Phys.* 1993;98:1372–7.
119. Becke AD. Density-functional thermochemistry. III. The role of exact exchange. *J Chem Phys.* 1993;98:5648–52.
120. Lee C, Yang W, Parr RG. Development of the Colle-Salvetti correlation-energy formula into a functional of the electron density. *Phys Rev B.* 1988;37:785–9.
121. Stephens PJ, Devlin FJ, Chabalowski CF, Frisch MJ. Ab initio calculation of vibrational absorption and circular dichroism spectra using density functional force fields. *J Phys Chem.* 1994;98:11623–7.
122. Becke AD. Density-functional thermochemistry. V. Systematic optimization of exchange-correlation functionals. *J Chem Phys.* 1997; 107:8554–60.
123. Hamprecht FA, Cohen AJ, Tozer DJ, Handy NC. Development and assessment of new exchange-correlation functionals. *J Chem Phys.* 1998;109:6264–71.
124. Adamo C, Barone V. Toward reliable density functional methods without adjustable parameters: the PBE0 model. *J Chem Phys.* 1999; 110:6158–70.
125. Lynch BJ, Fast PL, Harris M, Truhlar DG. Adiabatic connection for kinetics. *J Phys Chem A.* 2000;104:4811–5.
126. Zhao Y, Truhlar DG. The M06 suite of density functionals for main group thermochemistry, thermochemical kinetics, noncovalent interactions, excited states, and transition elements: two new functionals and systematic testing of four M06-class functionals and 12 other functionals. *Theor Chem Acc.* 2008;120:215–41.
127. Toulouse J, Colonna F, Savin A. Long-range-short-range separation of the electron-electron interaction in density-functional theory. *Phys Rev A.* 2004;70:062505.
128. Gill PMW, Adamson RD, Pople JA. Coulomb-attenuated exchange energy density functionals. *Mol Phys.* 1996;88:1005–9.
129. Iikura H, Tsuneda T, Yanai T, Hirao K. A long-range correction scheme for generalized-gradient-approximation exchange functionals. *J Chem Phys.* 2001;115:3540–4.
130. Yanai T, Tew DP, Handy NC. A new hybrid exchange-correlation functional using the Coulomb-attenuating method (CAM-B3LYP). *Chem Phys Lett.* 2004;393:51–7.
131. Peach MJ, Cohen AJ, Tozer DJ. Influence of Coulomb-attenuation on exchange–correlation functional quality. *Phys Chem Chem Phys.* 2006;8:4543–9.
132. Vydrov OA, Scuseria GE. Assessment of a long-range corrected hybrid functional. *J Chem Phys.* 2006;125:234109.
133. Vydrov OA, Heyd J, Krukau AV, Scuseria GE. Importance of short-range versus long-range Hartree–Fock exchange for the performance of hybrid density functionals. *J Chem Phys.* 2006;125:074106.
134. Chai JD, Head-Gordon M. Systematic optimization of long-range corrected hybrid density functionals. *J Chem Phys.* 2008;128:084106.
135. Heyd J, Scuseria GE, Ernzerhof M. Hybrid functionals based on a screened Coulomb potential. *J Chem Phys.* 2003;118:8207–15.
136. Krukau AV, Vydrov OA, Izmaylov AF, Scuseria GE. Influence of the exchange screening parameter on the performance of screened hybrid functionals. *J Chem Phys.* 2006;125:224106.
137. Frisch MJ, Trucks GW, Schlegel HB, Scuseria GE, Robb MA, Cheeseman JR, et al. Gaussian16 Revision B.01. Wallingford: Gaussian Inc; 2016.
138. Turney JM, Simonett AC, Parrish RM, Hohenstein EG, Evangelista F, Fermann JT, et al. Psi4: an open-source ab initio electronic structure program. *WIREs Comput Mol Sci.* 2012;2:556–65.

139. Schwalbe S, Fiedler L, Kraus J, Kortus J, Trepte K, Lehtola S. PyFLOSIC: python-based Fermi-Löwdin orbital self-interaction correction. *J Chem Phys.* 2020;153:084104.
140. Heaton RA, Harrison JG, Lin CC. Self-interaction correction for density-functional theory of electronic energy bands of solids. *Phys Rev B.* 1983;28:5992–6007.
141. Svane A, Gunnarsson O. Transition-metal oxides in the self-interaction-corrected density-functional formalism. *Phys Rev Lett.* 1990;65: 1148–51.
142. Szotek Z, Temmerman WM, Winter H. Application of the self-interaction correction to transition-metal oxides. *Phys Rev B.* 1993;47: 4029(R)–4032.
143. Stengel M, Spaldin NA. Self-interaction correction with Wannier functions. *Phys Rev B.* 2008;77:155106.
144. Shinde R, Yamijala SSRKC, Wong BM. Improved band gaps and structural properties from Wannier-Fermi-Löwdin self-interaction corrections for periodic systems. *J Phys Condens Matter.* 2021;33:115501.
145. Gräfenstein J, Kraka E, Cremer D. Effect of the self-interaction error for three-electron bonds: on the development of new exchange-correlation functionals. *Phys Chem Chem Phys.* 2004;6:1096–112.
146. Vydrov OA, Scuseria GE. Effect of the Perdew-Zunger self-interaction correction on the thermochemical performance of approximate density functionals. *J Chem Phys.* 2004;121:8187.
147. Vydrov OA, Scuseria GE. Ionization potentials and electron affinities in the Perdew-Zunger self-interaction corrected density-functional theory. *J Chem Phys.* 2005;122:184107.
148. Klüpfel S, Klüpfel P, Jónsson H. The effect of the Perdew-Zunger self-interaction correction to density functionals on the energetics of small molecules. *J Chem Phys.* 2012;137:124102.
149. Santra B, Perdew JP. Perdew-Zunger self-interaction correction: how wrong for uniform densities and large-Z atoms? *J Chem Phys.* 2019;150:174106.
150. Vydrov OA, Scuseria GE. Scaling down the Perdew-Zunger self-interaction correction in many-electron regions. *J Chem Phys.* 2006; 124:094108.
151. Ruzsinszky A, Perdew JP, Csonka GI, Vydrov OA, Scuseria GE. Density functionals that are one- and two- are not always many-electron self-interaction-free, as shown for H-2(+), He-2(+), LiH+, and Ne-2(+). *J Chem Phys.* 2007;126:104102.
152. Tsuneda T, Kamiya M, Hirao K. Regional self-interaction correction of density functional theory. *J Comput Chem.* 2003;24:1592–8.
153. Zope RR, Yamamoto Y, Diaz CM, Baruah T, Peralta JE, Jackson KA, et al. A step in the direction of resolving the paradox of Perdew-Zunger self-interaction correction. *J Chem Phys.* 2019;151:214108.
154. Bhattacharai P, Santra B, Wagle K, Yamamoto Y, Zope RR, Ruzsinszky A, et al. Exploring and enhancing the accuracy of interior-scaled Perdew-Zunger self-interaction correction. *J Chem Phys.* 2021;154:094105.
155. Bhattacharai P, Wagle K, Shahi C, Yamamoto Y, Romero S, Santra B, et al. A step in the direction of resolving the paradox of Perdew-Zunger self-interaction correction. II. Gauge consistency of the energy density at three levels of approximation. *J Chem Phys.* 2020;152: 214109.
156. Hui Yang Z, Pederson MR, Perdew JP. Full self-consistency in the Fermi-orbital self-interaction correction. *Phys Rev A.* 2017;95: 052505.
157. Pederson MR, Ruzsinszky A, Perdew JP. Self-interaction correction with unitary invariance in density functional theory. *J Chem Phys.* 2014;140:121103.
158. Diaz CM, Suryanarayana P, Xu Q, Baruah T, Pask JE, Zope RR. Implementation of Perdew-Zunger self-interaction correction in real space using Fermi-Löwdin orbitals. *J Chem Phys.* 2021;154:084112.
159. Karanovich A, Yamamoto Y, Jackson KA, Park K. Electronic structure of mononuclear cu-based molecule from density-functional theory with self-interaction correction. *J Chem Phys.* 2021;155:014106.
160. Wagle K, Santra B, Bhattacharai P, Shahi C, Pederson MR, Jackson KA, et al. Self-interaction correction in water-ion clusters. *J Chem Phys.* 2021;154:094302.
161. Akter S, Yamamoto Y, Zope RR, Baruah T. Static dipole polarizabilities of polyacenes using self-interaction-corrected density functional approximations. *J Chem Phys.* 2021;154:114305.
162. Akter S, Vargas JA, Sharkas K, Peralta JE, Jackson KA, Baruah T, et al. How well do self-interaction corrections repair the overestimation of static polarizabilities in density functional calculations? *Phys Chem Chem Phys.* 2021;23:18678–85.
163. Sharkas K, Wagle K, Santra B, Akter S, Zope RR, Baruah T, et al. Self-interaction error overbinds water clusters but cancels in structural energy differences. *Proc Natl Acad Sci.* 2020;117:11283–8.
164. Yamamoto Y, Romero S, Baruah T, Zope RR. Improvements in the orbitalwise scaling down of Perdew-Zunger self-interaction correction in many-electron regions. *J Chem Phys.* 2020;152:174112.
165. Kohut SV, Ryabinkin IG, Staroverov VN. Hierarchy of model Kohn-Sham potentials for orbital-dependent functionals: a practical alternative to the optimized effective potential method. *J Chem Phys.* 2014;140:18A535.
166. Diaz CM, Basurto L, Adhikari S, Yamamoto Y, Ruzsinszky A, Baruah T, et al. Self-interaction-corrected Kohn-Sham effective potentials using the density-consistent effective potential method. *J Chem Phys.* 2021;155:064109.
167. Krieger JB, Li Y, Iafrate GJ. Construction and application of an accurate local spin-polarized Kohn-Sham potential with integer discontinuity: exchange-only theory. *Phys Rev A.* 1992;45:101–26.
168. Diaz CM, Baruah T, Zope RR. Fermi-Löwdin-orbital self-interaction correction using the optimized-effective-potential method within the Krieger-Li-Iafrate approximation. *Phys Rev A.* 2021;103:042811.

169. Zhang YK, Yang WT. A challenge for density functionals: self-interaction error increases for systems with a noninteger number of electrons. *J Chem Phys*. 1998;109:2604–8.
170. Yang W, Zhang Y, Ayers PW. Degenerate ground states and a fractional number of electrons in density and reduced density matrix functional theory. *Phys Rev Lett*. 2000;84:5172–5.
171. Johnson ER, Otero-de-la-Roza A, Dale SG. Extreme density-driven delocalization error for a model solvated-electron system. *J Chem Phys*. 2013;139:184116.
172. Whittleton SR, Vazquez XAS, Isborn CM, Johnson ER. Density-functional errors in ionization potential with increasing system size. *J Chem Phys*. 2015;142:184106.
173. Janak JF. Proof that $\partial E/\partial n_i = \epsilon$ in density-functional theory. *Phys Rev B*. 1978;18:7165–8.
174. Blum V, Gehrke R, Hanke F, Havu P, Havu V, Ren X, et al. *Ab initio* molecular simulations with numeric atom-centered orbitals. *Comput Phys Commun*. 2009;180:2175–96.
175. Streetman BG, Banerjee S, et al. Solid state electronic devices. Vol 10. Upper Saddle River: Pearson/Prentice Hall; 2006.
176. Cohen AJ, Mori-Sánchez P, Yang W. Second-order perturbation theory with fractional charges and fractional spins. *J Chem Theory Comput*. 2009;5:786–92.
177. Paula Mori-Sánchez AJC, Yang W. Self-interaction-free exchange-correlation functional for thermochemistry and kinetics. *J Chem Phys*. 2006;124:091102.
178. Becke AD. Real-space post-Hartree-Fock correlation models. *J Chem Phys*. 2005;122:064101.
179. Schmidt T, Kraisler E, Makmal A, Kronik L, Kümmel S. A self-interaction-free local hybrid functional: accurate binding energies vis-à-vis accurate ionization potentials from Kohn-Sham eigenvalues. *J Chem Phys*. 2014;140:18A510.
180. Schmidt T, Kümmel S. One- and many-electron self-interaction error in local and global hybrid functionals. *Phys Rev B*. 2016;93:165120.
181. Kaupp M, Bahmann H, Arbuznikov AV. Local hybrid functionals: an assessment for thermochemical kinetics. *J Chem Phys*. 2007;127:194102.
182. Lonsdale DR, Goerigk L. The one-electron self-interaction error in 74 density functional approximations: a case study on hydrogenic mono- and dinuclear systems. *Phys Chem Chem Phys*. 2020;22:15805–30.
183. Stein T, Autschbach J, Govind N, Kronik L, Baer R. Curvature and frontier orbital energies in density functional theory. *J Phys Chem Lett*. 2012;3:3740–4.
184. Kronik L, Stein T, Refaelly-Abramson S, Baer R. Excitation gaps of finite-sized systems from optimally tuned range-separated hybrid functionals. *J Chem Theory Comput*. 2012;8:1515–31.
185. Kraisler E, Kronik L. Piecewise linearity of approximate Density Functionals revisited: implications for frontier orbital energies. *Phys Rev Lett*. 2013;110:126403.
186. Sun H, Autschbach J. Influence of the delocalization error and applicability of optimal functional tuning in density functional calculations of nonlinear optical properties of organic donor–acceptor chromophores. *ChemPhysChem*. 2013;14:2450–61.
187. Koppen JV, Hapka M, Modrzejewski M, Szczesniak MM, Chalasinski G. Density functional theory approach to gold-ligand interactions: separating true effects from artifacts. *J Chem Phys*. 2014;140:244313.
188. Autschbach J, Srebro M. Delocalization error and “functional tuning” in Kohn-Sham calculations of molecular properties. *Acc Chem Res*. 2014;47:2592–602.
189. Sivan Refaelly-Abramson MJ, Sharifzadeh S, Neaton JB, Kronik L. Solid-state optical absorption from optimally tuned time-dependent range-separated hybrid density functional theory. *Phys Rev B*. 2015;92:081204.
190. Sarkar S, Kronik L. Ionisation and (de-) protonation energies of gas-phase amino acids from an optimally tuned range-separated hybrid functional. *Mol Phys*. 2016;114:1218–24.
191. Brumboiu IE, Prokopiou G, Kronik L, Brena B. Valence electronic structure of cobalt phthalocyanine from an optimally tuned range-separated hybrid functional. *J Chem Phys*. 2017;147:044301.
192. Prokopiou G, Kronik L. Spin-state energetics of Fe complexes from an optimally tuned range-separated hybrid functional. *Chem A Eur J*. 2018;24:5173–82.
193. Manna AK, Refaelly-Abramson S, Reilly AM, Tkatchenko A, Neaton JB, Kronik L. Quantitative prediction of optical absorption in molecular solids from an optimally tuned screened range-separated hybrid functional. *J Chem Theory Comput*. 2018;14:2919–29.
194. Prokopiou G, Autschbach J, Kronik L. Assessment of the performance of optimally tuned range-separated hybrid Functionals for nuclear magnetic shielding calculations. *Adv Theory Simul*. 2020;3:2000083.
195. Wing D, Ohad G, Haber JB, Filip MR, Gant SE, Neaton JB, et al. Band gaps of crystalline solids from Wannier-localization-based optimal tuning of a screened range-separated hybrid functional. *Proc Nat Acad Sci*. 2021;118:e2104556118.
196. Koerzdoerfer T, Sears JS, Sutton C, Bredas JL. Long-range corrected hybrid Functionals for pi-conjugated systems: dependence of the range-separation parameter on conjugation length. *J Chem Phys*. 2011;135:204107.
197. Korzdorfer T, Parrish RM, Marom N, Sears JS, Sherrill CD, Bredas JL. Assessment of the performance of tuned range-separated hybrid density functionals in predicting accurate quasiparticle spectra. *Phys Rev B*. 2012;86:205110.
198. Garrett K, Sosa Vazquez XA, Egri SB, Wilmer J, Johnson LE, Robinson BH, et al. Optimum exchange for calculation of excitation energies and hyperpolarizabilities of organic electro-optic chromophores. *J Chem Theory Comput*. 2014;10:3821–31.
199. Li C, Zheng X, Cohen AJ, Mori-Sánchez P, Yang W. Local scaling correction for reducing delocalization error in density functional approximations. *Phys Rev Lett*. 2015;114:053001.

200. Li C, Zheng X, Su NQ, Yang W. Localized orbital scaling correction for systematic elimination of delocalization error in density functional approximations. *Nat Sci Rev.* 2018;5:203–15.
201. Su NQ, Mahler A, Yang W. Preserving symmetry and degeneracy in the localized orbital scaling correction approach. *J Phys Chem Lett.* 2020;11:1528–35.
202. Mei Y, Chen Z, Yang W. Self-consistent calculation of the localized orbital scaling correction for correct electron densities and energy-level alignments in Density functional theory. *J Phys Chem Lett.* 2020;11:10269–77.
203. Mei Y, Yang N, Yang W. Describing polymer polarizability with localized orbital scaling correction in density functional theory. *J Chem Phys.* 2021;154:054302.
204. Polo V, Gräfenstein J, Kraka E, Cremer D. Influence of the self-interaction error on the structure of the DFT exchange hole. *Chem Phys Lett.* 2002;352:469–78.
205. Gunnarsson O, Lundqvist BI. Exchange and correlation in atoms, molecules, and solids by the spin-density-functional formalism. *Phys Rev B.* 1976;13(10):4274–98.
206. Buijse MA, Baerends EJ. An approximate exchange-correlation hole density as a functional of the natural orbitals. *Mol Phys.* 2002;100:401–21.
207. Becke AD. Hartree-Fock exchange energy of an inhomogeneous electron gas. *Int J Quantum Chem.* 1983;23:1915–22.
208. Janesko BG, Proynov E, Scalmani G, Frisch MJ. Long-range-corrected rung 3.5 density functional approximations. *J Chem Phys.* 2018;148(10):104112.
209. Kim MC, Sim E, Burke K. Understanding and reducing errors in density functional calculations. *Phys Rev Lett.* 2013;111:073003.
210. Kim MC, Sim E, Burke K. Ions in solution: Density corrected density functional theory (DC-DFT). *J Chem Phys.* 2014;140:18A528.
211. Kim MC, Park H, Son S, Sim E, Burke K. Improved DFT potential energy surfaces via improved densities. *J Phys Chem Lett.* 2015;6:3802–7.
212. Wasserman A, Nafziger J, Jiang K, Kim MC, Sim E, Burke K. The importance of being inconsistent. *Ann Rev Phys Chem.* 2017;68:555–81.
213. Sim E, Song S, Burke K. Quantifying density errors in DFT. *J Phys Chem Lett.* 2018;9:6385–92.
214. Vuckovic S, Song S, Kozlowski J, Sim E, Burke K. Density functional analysis: the theory of density-corrected DFT. *J Chem Theory Comput.* 2019;15:6636–46.
215. Song S, Vuckovic S, Sim E, Burke K. Density sensitivity of empirical Functionals. *J Phys Chem Lett.* 2021;12:800–7.
216. Santra G, Martin JM. What types of chemical problems benefit from density-corrected DFT? A probe using an extensive and chemically diverse test suite. *J Chem Theory Comput.* 2021;17:1368–79.
217. Dasgupta S, Lambros E, Perdew JP, Paesani F. Elevating density functional theory to chemical accuracy for water simulations through a density-corrected many-body formalism. *Nat Comm.* 2021;12:6359.
218. Grimme S, Ehrlich S, Goerigk L. Effect of the damping function in dispersion corrected density functional theory. *J Comput Chem.* 2011;32:1456–65.
219. Bauzá A, Alkorta I, Frontera A, Elguero J. On the reliability of pure and hybrid DFT methods for the evaluation of halogen, chalcogen, and pnictogen bonds involving anionic and neutral electron donors. *J Chem Theory Comput.* 2013;9:5201–10.
220. Karton A, Rabinovich E, Martin JML. W4 theory for computational thermochemistry: in pursuit of confident sub-kJ/mol predictions. *J Chem Phys.* 2006;125:144108.
221. Lommers JPM, Stone AJ, Taylor R, Allen FH. The nature and geometry of intermolecular interactions between halogens and oxygen or nitrogen. *J Am Chem Soc.* 1996;118:3108–16.
222. Metrangolo P, Neukirch H, Pilati T, Resnati G. Halogen bonding based recognition processes: A world parallel to hydrogen bonding. *Acc Chem Res.* 2005;38:386–95.
223. Clark T, Hennemann M, Murray JS, Politzer P. Halogen bonding: the σ -hole. *J Mol Model.* 2007;13:291–6.
224. Politzer P, Murray JS, Clark T. Halogen bonding: an electrostatically-driven highly directional noncovalent interaction. *Phys Chem Chem Phys.* 2010;12:7748–57.
225. Murray JS, Lane P, Politzer P. Simultaneous σ -hole and hydrogen bonding by sulfur- and selenium-containing heterocycles. *Int J Quantum Chem.* 2008;108:2770–81.
226. Pascoe DJ, Ling KB, Cockcroft SL. The origin of chalcogen-bonding interactions. *J Am Chem Soc.* 2017;139:15160–7.
227. Vogel L, Wonner P, Huber SM. Chalcogen bonding: an overview. *Angew Chem Int Ed.* 2018;58:1880–91.
228. Řezáč J, Riley KE, Hobza P. Benchmark calculations of noncovalent interactions of halogenated molecules. *J Chem Theory Comput.* 2012;8:4285–92.
229. Kozuch S, Martin JML. Halogen bonds: benchmark and theoretical analysis. *J Chem Theory Comput.* 2013;9:1918–31.
230. Sonnenberg JL, Schlegel HB, Hratchian HP. Spin contamination in inorganic chemistry calculations. In: Solomon EI, Scott RA, King RB, editors. Computational inorganic and bioinorganic chemistry. Hoboken, NJ: Wiley; 2009. p. 173–86.
231. Liu F, Kulik HJ. Impact of approximate DFT density delocalization error on potential energy surfaces in transition metal chemistry. *J Chem Theory Comput.* 2020;16:264–77.
232. Johnson ER, Salamone M, Bietti M, DiLabio GA. Modeling non-covalent radical-molecule interactions using conventional density-functional theory: beware erroneous charge transfer. *J Phys Chem A.* 2013;117:947–52.
233. Smith JM, Alahmadi YJ, Rowley CN. Range-separated DFT functionals are necessary to model Thio-Michael additions. *J Chem Theory Comput.* 2013;9:4860–5.

234. Awoonor-Williams E, Isley WC, Dale SG, Johnson ER, Yu H, Becke AD, et al. Quantum chemical methods for modeling covalent modification of biological thiols. *J Comput Chem*. 2020;41:427–38.
235. Marshall MS, Burns LA, Sherrill CD. Basis set convergence of the coupled-cluster correction, delta-MP2-CCSD(T): best practices for benchmarking non-covalent interactions and the attendant revision of the S22, NBC10, HBC6, and HSG databases. *J Chem Phys*. 2011;135:194102.
236. Pernal K, Podeszwa R, Patkowski K, Szalewicz K. Dispersionless density functional theory. *Phys Rev Lett*. 2009;103:263201.
237. Sun J, Xiao B, Fang Y, Haunschmid R, Hao P, Ruzsinszky A, et al. Density functionals that recognize covalent, metallic, and weak bonds. *Phys Rev Lett*. 2013;111:106401.
238. Peng H, Yang ZH, Perdew JP, Sun J. Versatile van der Waals Density functional based on a meta-generalized gradient approximation. *Phys Rev X*. 2016;6:041005.
239. Adhikari S, Tang H, Neupane B, Ruzsinszky A, Csonka GI. Molecule-surface interaction from van der Waals-corrected semilocal density functionals: the example of thiophene on transition-metal surfaces. *Phys Rev Mater*. 2020;4:025005.
240. Johnson ER, Mori-Sánchez P, Yang W. Delocalization errors in density functionals and implications for main-group thermochemistry. *J Chem Phys*. 2008;129:204112.
241. Řezáč J, Riley KE, Hobza P. S66: a well-balanced database of benchmark interaction energies relevant to biomolecular structures. *J Chem Theory Comput*. 2011;7:2427–38.
242. DiLabio GA, Johnson ER, Otero-de-la RA. Performance of conventional and dispersion-corrected density-functional theory methods for hydrogen bonding interaction energies. *Phys Chem Chem Phys*. 2013;15:12821–8.
243. Temelso B, Archer KA, Shields GC. Benchmark structures and binding energies of small water clusters with anharmonicity corrections. *J Phys Chem A*. 2011;115:12034–46.
244. Grimme S, Antony J, Ehrlich S, Krieg H. A consistent and accurate ab initio parametrization of density functional dispersion correction (DFT-D) for the 94 elements H-Pu. *J Chem Phys*. 2010;132:154104.
245. Tkatchenko A, Scheffler M. Accurate molecular van der Waals interactions from ground-state electron density and free-atom reference data. *Phys Rev Lett*. 2009;102:073005.
246. Tkatchenko A, DiStasio RA, Car R, Scheffler M. Accurate and efficient method for many-body van der Waals interactions. *Phys Rev Lett*. 2012;108:236402.
247. Ambrosetti A, Reilly AM, DiStasio RA Jr, Tkatchenko A. Long-range correlation energy calculated from coupled atomic response functions. *J Chem Phys*. 2014;140:18A508.
248. Johnson ER, Becke AD. A post-Hartree-Fock model of intermolecular interactions: inclusion of higher-order corrections. *J Chem Phys*. 2006;124:174104.
249. Otero-de-la-Roza A, Johnson ER. Van der Waals interactions in solids using the exchange-hole dipole moment. *J Chem Phys*. 2012;136:174109.
250. Otero-de-la-Roza A, Johnson ER. Non-covalent interactions and thermochemistry using XDM-corrected hybrid and range-separated hybrid density functionals. *J Chem Phys*. 2013;138:204109.
251. Johnson ER. The exchange-hole dipole moment dispersion model. In: Otero-de-la-Roza A, DiLabio GA, editors. Non-covalent interactions in quantum chemistry and physics. Amsterdam, Netherlands: Elsevier; 2017. p. 169–94.
252. Lee K, Murray ÉD, Kong L, Lundqvist BI, Langreth DC. Higher-accuracy van der Waals density functional. *Phys Rev B*. 2010;82:081101.
253. Schröder E, Cooper VR, Berland K, Lundqvist BI, Hyldgaard P, Thonhauser T. The vdW-DF family of nonlocal exchange-correlation functionals. In: Otero-de-la-Roza A, DiLabio GA, editors. Non-covalent interactions in quantum chemistry and physics. Amsterdam, Netherlands: Elsevier; 2017. p. 241–74.
254. Sabatini R, Gorni T, de Gironcoli S. Nonlocal van der Waals density functional made simple and efficient. *Phys Rev B*. 2013;87:041108.
255. Piquemal JP, Marquez A, Parisel O, Giessner-Prettre C. A CSOV study of the difference between HF and DFT intermolecular interaction energy values: the importance of the charge transfer contribution. *J Comput Chem*. 2005;26:1052–62.
256. Zhao Y, Lynch BJ, Truhlar DG. Doubly hybrid meta DFT: new multi-coefficient correlation and density functional methods for thermochemistry and thermochemical kinetics. *J Phys Chem A*. 2004;108:4786–91.
257. Grimme S. Semiempirical hybrid density functional with perturbative second-order correlation. *J Chem Phys*. 2006;124:034108.
258. Tarnopolsky A, Karton A, Sertchook R, Vuzman D, Martin JML. Double-hybrid functionals for thermochemical kinetics. *J Phys Chem A*. 2008;112:3–8.
259. Zhang Y, Xu X III, WAG. Doubly hybrid density functional for accurate descriptions of nonbond interactions, thermochemistry, and thermochemical kinetics. *Proc Natl Acad Sci*. 2009;106:4963–8.
260. Brémond E, Adamo C. Seeking for parameter-free double-hybrid functionals: the PBE0-DH model. *J Chem Phys*. 2011;135:024106.
261. Sancho-García JC, Adamo C. Double-hybrid density functionals: merging wavefunction and density approaches to get the best of both worlds. *Phys Chem Chem Phys*. 2013;15:14581–94.
262. Goerigk L, Grimme S. Efficient and accurate double-hybrid-meta-GGA density functionals—evaluation with the extended GMTKN30 database for general main group thermochemistry, kinetics, and noncovalent interactions. *J Chem Theory Comput*. 2010;7:291–309.
263. Menon AS, Radom L. Consequences of spin contamination in unrestricted calculations on open-shell species: effect of Hartree-Fock and Møller-Plesset contributions in hybrid and double-hybrid density functional theory approaches. *J Phys Chem A*. 2008;112:13225–30.

264. Thompson LM, Hratchian HP. Spin projection with double hybrid density functional theory. *J Chem Phys.* 2014;141:034108.
265. Peverati R, Head-Gordon M. Orbital optimized double-hybrid density functionals. *J Chem Phys.* 2013;139:024110.
266. Grüneis A, Marsman M, Harl J, Schimka L, Kresse G. Making the random phase approximation to electronic correlation accurate. *J Chem Phys.* 2009;131:154115.
267. Paier J, Janesko BG, Henderson TM, Scuseria GE, Grüneis A, Kresse G. Hybrid functionals including random phase approximation correlation and second-order screened exchange. *J Chem Phys.* 2010;132:094103.
268. Eshuis H, Bates JE, Furche F. Electron correlation methods based on the random phase approximation. *Theor Chem Acc.* 2012;131:1084.
269. Mezei PD, Csonka GI, Ruzsinszky A, Kállay M. Construction and application of a new dual-hybrid random phase approximation. *J Chem Theory Comput.* 2015;11:4615–26.
270. Grimme S, Steinmetz M. A computationally efficient double hybrid density functional based on the random phase approximation. *Phys Chem Chem Phys.* 2016;18:20926–37.
271. Zhang IY, Xu X. Simultaneous attenuation of both self-interaction error and nondynamic correlation error in density functional theory: a spin-pair distinctive adiabatic-connection approximation. *J Phys Chem Lett.* 2019;10:2617–23.
272. Janesko BG. Rung 3.5 density functionals. *J Chem Phys.* 2010;133:104103.
273. Janesko BG. Rung 3.5 density functionals: another step on Jacob's ladder. *Int J Quantum Chem.* 2012;113:83–8.
274. Janesko BG, Scalmani G, Frisch MJ. Practical auxiliary basis implementation of rung 3.5 functionals. *J Chem Phys.* 2014;141:034103.
275. Verma P, Janesko BG, Wang Y, He X, Scalmani G, Frisch MJ, et al. M11plus: a range-separated hybrid meta functional with both local and Rung-3.5 correlation terms and high across-the-board accuracy for chemical applications. *J Chem Theory Comput.* 2019;15:4804–15.
276. Dudarev SL, Botton GA, Savrasov SY, Humphreys CJ, Sutton AP. Electron-energy-loss spectra and the structural stability of nickel oxide: an LSDA+U study. *Phys Rev B.* 1998;57:1505–9.
277. Jain A, Hautier G, Ong SP, Moore CJ, Fischer CC, Persson KA, et al. Formation enthalpies by mixing GGA and GGA+U calculations. *Phys Rev B.* 2011;84:045115.
278. Himmeloglu B, Floris A, de Gironcoli S, Cococcioni M. Hubbard-corrected DFT energy functionals: the LDA+U description of correlated systems. *Int J Quantum Chem.* 2014;114:14–49.
279. Kulik HJ. Treating electron over-delocalization with the DFT+U method. *J Chem Phys.* 2015;142:240901.
280. Beridze G, Birnie A, Koniski S, Ji Y, Kowalski PM. DFT+U as a reliable method for efficient ab initio calculations of nuclear materials. *Prog Nucl Energy.* 2016;92:142–6.
281. Bajaj A, Kulik HJ. Molecular DFT+U: a transferable, low-cost approach to eliminate delocalization error. *J Phys Chem Lett.* 2021;12:3633–40.
282. Bajaj A, Kulik HJ. Eliminating delocalization error to improve heterogeneous catalysis predictions with molecular DFT+ U. *J Chem Theory Comput.* 2021;18:1142–55.
283. Jing W, Liu M, Wen J, Ning L, Yin M, Duan CK. First-principles study of Ti-doped sapphire. I. Formation and optical transition properties of titanium pairs. *Phys Rev B.* 2021;104:165103.
284. Tran F, Blaha P. Accurate band gaps of semiconductors and insulators with a semilocal exchange-correlation potential. *Phys Rev Lett.* 2009;102:226401.
285. Becke AD, Johnson ER. A simple effective potential for exchange. *J Chem Phys.* 2006;124:221101.
286. Koller D, Tran F, Blaha P. Merits and limits of the modified Becke-Johnson exchange potential. *Phys Rev B.* 2011;83:195134.
287. Koller D, Tran F, Blaha P. Improving the modified Becke-Johnson exchange potential. *Phys Rev B.* 2012;85:155109.
288. Camargo-Martínez JA, Baquero R. Performance of the modified Becke-Johnson potential for semiconductors. *Phys Rev B.* 2012;86:195106.
289. Jiang H. Band gaps from the Tran-Blaha modified Becke-Johnson approach: a systematic investigation. *J Chem Phys.* 2013;138:134115.
290. Rauch T, Marques MAL, Botti S. Local modified Becke-Johnson exchange-correlation potential for interfaces, surfaces, and two-dimensional materials. *J Chem Theory Comput.* 2020;16:2654–60.
291. Rauch T, Marques MAL, Botti S. Accurate electronic band gaps of two-dimensional materials from the local modified Becke-Johnson potential. *Phys Rev B.* 2020;101:245163.
292. Perdew JP, Staroverov VN, Tao J, Scuseria GE. Density functional with full exact exchange, balanced nonlocality of correlation, and constraint satisfaction. *Phys Rev A.* 2008;78:052513.
293. Proynov E, Kong J. Correcting the charge delocalization error of density functional theory. *J Chem Theory Comput.* 2021;17:4633–8.
294. Přečechtělová J, Bahmann H, Kaupp M, Ernzerhof M. A non-empirical correlation factor model for the exchange-correlation energy. *J Chem Phys.* 2014;141:111102.
295. Přečechtělová J, Bahmann H, Kaupp M, Ernzerhof M. Design of exchange-correlation functionals through the correlation factor approach. *J Chem Phys.* 2015;143:144102.
296. Wang R, Zhou Y, Ernzerhof M. Construction of self-interaction-corrected exchange-correlation functionals within the correlation factor approach. *J Chem Phys.* 2019;151:194102.
297. Jaramillo J, Scuseria GE. Local hybrid functionals. *J Chem Phys.* 2003;118:1068–73.
298. Janesko BG, Scuseria GE. Local hybrid functionals based on density matrix products. *J Chem Phys.* 2007;127:164117.

299. Arbuznikov AV, Kaupp M. Local hybrid exchange-correlation functionals based on the dimensionless density gradient. *Chem Phys Lett.* 2007;440:160–8.
300. Arbuznikov AV, Bahmann H, Kaupp M. Local hybrid functionals with an explicit dependence on spin polarization. *J Phys Chem A.* 2009;113:11898–906.
301. Johnson ER. Local-hybrid functional based on the correlation length. *J Chem Phys.* 2014;141:124120.
302. de Silva P, Corminboeuf C. Local hybrid functionals with orbital-free mixing functions and balanced elimination of self-interaction error. *J Chem Phys.* 2015;142:074112.
303. Haasler M, Maier TM, Grotjahn R, Gückel S, Arbuznikov AV, Kaupp M. A local hybrid functional with wide applicability and good balance between (de)localization and left-right correlation. *J Chem Theory Comput.* 2020;16:5645–57.
304. Becke AD. Correlation energy of an inhomogeneous electron gas - a coordinate-space model. *J Chem Phys.* 1988;88:1053–62.
305. Dale SG, Johnson ER, Becke AD. Interrogating the Becke'05 density functional for non-locality information. *J Chem Phys.* 2017;147:154103.
306. Becke AD. Density-functional theory versus density-functional fits. *J Chem Phys.* 2022;156:214101.
307. Kirkpatrick J, McMorrow B, Turban DH, Gaunt AL, Spencer JS, Matthews AG, et al. Pushing the frontiers of density functionals by solving the fractional electron problem. *Science.* 2021;374:1385–9.
308. Gould T, Dale S. Poisoning density functional theory with benchmark sets of difficult systems. *Phys Chem Chem Phys.* 2022;24:6398–403.
309. Ramakrishnan R, Dral PO, Rupp M, Von Lilienfeld OA. Quantum chemistry structures and properties of 134 kilo molecules. *Sci Data.* 2014;1:1–7.
310. Kim H, Park JY, Choi S. Energy refinement and analysis of structures in the QM9 database via a highly accurate quantum chemical method. *Sci Data.* 2019;6:1–8.
311. Perdew JP. Artificial intelligence “sees” split electrons. *Science.* 2021;374:1322–3.

How to cite this article: Bryenton KR, Adeleke AA, Dale SG, Johnson ER. Delocalization error: The greatest outstanding challenge in density-functional theory. *WIREs Comput Mol Sci.* 2023;13(2):e1631. <https://doi.org/10.1002/wcms.1631>